Analysis of hindlimb muscle moment arms in *Tyrannosaurus rex* using a three-dimensional musculoskeletal computer model: implications for stance, gait, and speed

John R. Hutchinson, Frank C. Anderson, Silvia S. Blemker, and Scott L. Delp

Abstract.—Muscle moment arms are important determinants of muscle function; however, it is challenging to determine moment arms by inspecting bone specimens alone, as muscles have curvilinear paths that change as joints rotate. The goals of this study were to (1) develop a three-dimensional graphics-based model of the musculoskeletal system of the Cretaceous theropod dinosaur *Tyrannosaurus rex* that predicts muscle-tendon unit paths, lengths, and moment arms for a range of limb positions; (2) use the model to determine how the *T. rex* hindlimb muscle moment arms varied between crouched and upright poses; (3) compare the predicted moment arms with previous assessments of muscle function in dinosaurs; (4) evaluate how the magnitudes of these moment arms compare with those in other animals; and (5) integrate these findings with previous biomechanical studies to produce a revised appraisal of stance, gait, and speed in *T. rex*. The musculoskeletal model includes ten degrees of joint freedom (flexion/extension, ab/adduction, or medial/lateral rotation) and 33 main muscle groups crossing the hip, knee, ankle, and toe joints of each hindlimb. The model was developed by acquiring and processing bone geometric data, defining joint rotation axes, justifying muscle attachment sites, and specifying muscle-tendon geometry and paths. Flexor and extensor muscle moment arms about all of the main limb joints were estimated, and limb orientation was statically varied to characterize how the muscle moment arms changed. We used sensitivity analysis of uncertain parameters, such as muscle origin and insertion centroids, to determine how much our conclusions depend on the muscle reconstruction we adopted. This shows that a specific amount of error in the reconstruction (e.g., position of muscle origins) can have a greater, lesser, similar, or no effect on the moment arms, depending on complex interactions between components of the musculoskeletal geometry. We found that more upright poses would have improved mechanical advantage of the muscles considerably. Our analysis shows that previously assumed moment arm values were generally conservatively high. Our results for muscle moment arms are generally lower than the values predicted by scaling data from extant taxa, suggesting that *T. rex* did not have the allometrically large muscle moment arms that might be expected in a proficient runner. The information provided by the model is important for determining how *T. rex* stood and walked, and how the muscles of a 4000–7000 kg biped might have worked in comparison with extant bipeds such as birds and humans. Our model thus strengthens the conclusion that *T. rex* was not an exceptionally fast runner, and supports the inference that more upright (although not completely columnar) poses are more plausible for *T. rex*. These results confirm general principles about the relationship between size, limb orientation, and locomotor mechanics: exceptionally big animals have a more limited range of locomotor abilities and tend to adopt more upright poses that improve extensor muscle effective mechanical advantage. This model builds on previous phylogenetically based muscle reconstructions and so moves closer to a fully dynamic, three-dimensional model of stance, gait, and speed in *T. rex*.

John R. Hutchinson,* Frank C. Anderson, Silvia S. Blemker, and Scott L. Delp. Biomechanical Engineering Division, Department of Mechanical Engineering, Stanford University, Stanford, California 94305-4038. E-mail: jrhutch@rvc.ac.uk
*Present address: Structure and Motion Laboratory, The Royal Veterinary College, University of London, Hatfield, Hertfordshire AL9 7TA, United Kingdom

Introduction

A major determinant of skeletal muscle function in a vertebrate body is its moment arm (or lever arm) about a given joint. Muscles with larger moment arms generate a greater moment about a joint for a given level of muscle force. This generally reduces the absolute amount of force that the muscle must generate to balance an external load. Muscles with large moment arms also undergo greater length changes for a given joint motion and shorten at a higher velocity for a given joint angular velocity (e.g., Lieber 1997; Rome 1998). The force-generating capacity of a muscle depends on its length and velocity (Zajac 1989), so moment arms have major effects on

muscle force output (e.g., Gans and De Vree 1987; Lieber 1992; Van Leeuwen 1992; Raikova and Prilutsky 2001). For all these reasons, researchers interested in understanding how extinct animals stood and moved have investigated the moment arms of muscles involved in such behaviors (e.g., Charig 1972; Russell 1972; Blanco and Mazetta 2001; Blob 2001; Hutchinson and Garcia 2002; Sellers et al. 2003; Hutchinson 2004a,b).

Muscle moment arms can be measured as the smallest distance between the line of action of a muscle-tendon complex and the center of rotation of a joint (the popular ''geometric method''), or as the change in length of a tendon per unit of joint rotation (the ''virtual work'' or ''tendon excursion method;'' An et al. 1984; Pandy 1999). Despite the simplicity of this definition, measuring or computing moment arms can be difficult. The paths (three-dimensional geometric course) that muscles follow and hence their moment arm values have been shown to often vary greatly with the joint angles (between two body segments) that are adopted (Spoor and Van Leeuwen 1992; Buford et al. 1997; Delp et al. 1999; Pandy 1999; Thorpe et al. 1999; Arnold et al. 2000; Arnold and Delp 2001; Kargo and Rome 2002; Brown et al. 2003a,b; Krevolin et al. 2004; Maganaris 2004). Thus limb orientation, or more informally the ''pose,'' (i.e., any set of joint angles) influences muscle moment arms and thereby affects the mechanics of body support. This dependence of moment arms on limb orientation has been studied extensively in the human musculoskeletal system. Biomechanical engineers studying human locomotor function have developed experimental (e.g., An et al. 1984; Buford et al. 1997; Krevolin et al. 2004; Maganaris 2004) and computer visualization tools to quantify accurately the relationship of muscle moment arms to joint angles (e.g., Delp et al. 1990, 1999; Pandy 1999). However, to our knowledge, no studies of extinct vertebrates have carefully investigated the variation in muscle moment arms with body position.

As a case study in how to model musculoskeletal function in extinct animals, here we constructed and used a computer model of the hindlimbs of one of the largest theropod (bipedal carnivorous) dinosaurs, *Tyrannosaurus rex*, to calculate what its hindlimb muscle moment arms might have been, how the moment arms might have varied with limb orientation, how the moment arms compare with previous assessments of muscle function in dinosaurs generally, and how the magnitudes of these moment arms compare with those in other animals. Furthermore, because muscle reconstructions are inferences with a certain degree of error (Bryant and Seymour 1990), we analyze how much variations of muscle attachment points (e.g., centroids of muscle origins) affect our results. These questions are of interest because the stance, gait, and speed of *T. rex* are controversial (Osborn 1916; Lambe 1917; Newman 1970; Hotton 1980; Thulborn 1982, 1989, 1990; Tarsitano 1983; Bakker 1986, 2002; Paul 1988, 1998; Molnar and Farlow 1990; Christiansen 1999; Hutchinson and Garcia 2002; Leahy 2002; Hutchinson 2004b). Like most dinosaurs, *T. rex* had a large pelvis, so the paths of many pelvic muscles were far removed from the hip joint. Hence it might be expected that many of those muscles could have had moment arms that varied substantially with limb orientation. Furthermore, the prominence of some features related to muscle moment arms, such as the fourth trochanter of the femur (for hip extensors), the cnemial crest on the cranial side of the proximal tibia (for knee extensors), and the ''hypotarsus''-like protuberances on the caudal side of the proximal metatarsus (for ankle extensors) have led some to assume high effective mechanical advantage and hence large moment arms for the associated muscles (Bakker 1986; Paul 1988, 1998; also see Molnar and Farlow 1990; Hutchinson 2004b). Yet without quantifying those moment arms and comparing them to values in other animals (especially those in which a correlation can be established between moment arms and locomotor behavior), such qualitative anatomical assessments have unclear relevance for inferences of locomotor function. Biomechanical models have the advantage of quantitatively assessing the functional consequences of anatomical specializations, facilitating explicit comparisons among both muscles and taxa. Although we focus mainly here on flexion/extension moment

arms, our model is fully three-dimensional unlike previous, simpler 2D biomechanical models (Hutchinson and Garcia 2002; Hutchinson 2004a,b) and hence is a major step toward anatomically realistic dynamic simulation of locomotion in *Tyrannosaurus*.

Hutchinson and Garcia (2002; also Hutchinson 2004a,b) used muscle moment arms to calculate how large the muscles of *T. rex* and other animals would have to be to exert the ground reaction forces involved in fast running, concluding that the required muscle masses were too high to enable rapid running ($\sim$11–20 m s^{-1}) in *T. rex*. However, they entered constant moment arm values, noting that the numbers they used were likely overestimates, particularly for more crouched poses. We thus compare our more realistic estimates of moment arms with the values they assumed to see if their conclusions might have differed. We synthesize this information with the literature to produce a revised evaluation of the possible stance, gait, and speed of *T. rex*. We aim to make this study explicit enough that others interested in modeling musculoskeletal function in extinct animals could follow our approach to construct and study their own models of other animals, or even test our conclusions for *T. rex*.

Methods

We describe our procedure for developing the *Tyrannosaurus* model in five steps: (1) bone geometry acquisition (digitization, image processing, and importation into biomechanics software), (2) joint axis estimation, (3) muscle reconstruction, (4) muscle path specification, and (5) moment arm calculation.

Bone Geometry Acquisition.—The first step in producing a biomechanical model of a chosen extinct animal is selecting the best specimen for the purposes of the study. Museum of the Rockies specimen MOR 555 is a fairly complete adult individual of *Tyrannosaurus*. We chose to model this specimen because of its good preservation and the accessibility of a sufficiently large digitizing system at the museum to acquire its three-dimensional bone geometry. We digitized the pelvis, femur, tibia, fibula, astragalus, calcaneum, distal tarsals, and metatarsals II-IV. This procedure is

detailed in Appendix 1. Measurements of the phalanges and metatarsals I and V were taken so their geometry could be considered in the 3-D model, but for simplicity they were not digitized. We acquired 3-D computer images of the actual bones that were suitably simple for use in biomechanics software but also realistically representative of bone morphology in life. Figure 1 shows the original bones and their computerized representations.

3-D Computer Model: Joint Axis Estimation.—The biomechanical modeling software used in this study was Software for Interactive Musculoskeletal Modeling (SIMM; Musculographics, Inc., Chicago). This software, developed for modeling locomotor function, pathology, and therapy (e.g., Delp and Zajac 1992; Delp and Loan 1995, 2000), has been shown to produce accurate results for a variety of taxa including humans (Delp et al. 1990, 1999; Arnold et al. 2000), cockroaches (Full and Ahn 1995), frogs (Kargo and Rome 2002; Kargo et al. 2002), cats (Keshner et al. 1997), horses (Brown et al. 2003a,b), and a variety of birds (Hutchinson et al. unpublished data). To connect the bone files into an articulated, movable limb in the musculoskeletal model, joints between adjacent limbs were created by specifying both centers of joint rotation and directions of joint axes. This was done for the hip, knee, ankle, and metatarsophalangeal joints (Fig. 2), which joined the pelvis to femur, femur to tibia, tibia to metatarsus (including tarsals), and metatarsus to pes, respectively. The methodology used for this procedure is detailed in Appendix 2. Ranges of joint motion allowed in the model are in Table 1. The accuracy of these joint axes is dependent on the preservation of the bones, our processing of the bone images to correct preservational artifacts, the quality with which the polygonal representations of the bones were constructed, and our assumptions about the displacements of joint axes caused by soft tissues such as cartilage (relative to bone surfaces alone); see Appendix 2 for details. The potential error is presumably small enough to avoid changing our conclusions but deserves separate investigation in the future, perhaps with experimental studies in extant animals.

Muscle Reconstruction.—Muscles that have

the same rough positions and connections in extant archosaurs (crocodiles and birds) can reasonably be inferred to have had the same features in extinct dinosaurs such as *Tyrannosaurus* (Witmer 1995) and placed into a musculoskeletal model with confidence. Luckily this is the case for most muscles in extinct dinosaurs, with some exceptions (see ''Sensitivity Analysis'' below). Carrano and Hutchinson (2002; based on a comprehensive survey of sauropsid hindlimb myology and osteology by Hutchinson 2001a,b; Hutchinson 2002) have already used the Extant Phylogenetic Bracket approach (Witmer 1995) to present the least speculative (most parsimonious) reconstruction of the gross hindlimb musculature of *Tyrannosaurus*, so our treatment here focuses on how the muscles were positioned and analyzed in the model. A total of 33 major muscle groups consisting of 37 ''muscles'' (muscle-tendon units; four groups were split into two parts each) were placed in the model, representing all major hindlimb muscle groups. Appendix 3 elaborates on this approach. The abbreviations used here for the muscles and the locations of their origins and insertions are listed in Tables 2 and 3. These initial locations were chosen as the approximate centroids of the muscle attachments, estimated from muscle scars when present, or when not present estimated by comparison with the relative positions of these muscles in extant Reptilia (including Aves). In the Discussion, we examine how much any potential inaccuracy in estimating these centroids of origin and insertion might affect our results.

Muscle Path Specification.—With the muscles connected from origin to insertion as outlined in Tables 2 and 3 and the limbs posed in a reference position (Fig. 2), it might seem that our work would be done and muscle moment arms could be calculated in a straightforward manner, but this is far from the case. Simple visualization of those ''raw'' muscle paths shows that many of those paths (particularly for the hip muscles) would be sweeping through unrealistically large arcs, passing through other muscles or even bones. Thus a straight-line approach (for example as shown by Charig [1972] and Russell [1972]) for quantifying muscle moment arms would be unre-

alistic. We needed to make an additional set of assumptions to constrain the muscle-tendon unit lines of action into biologically realistic paths. We did this by introducing ''via points''—points through which the muscle was constrained to always act (Delp et al. 1990; Delp and Loan 1995 (Appendix 4) and wrapping surfaces (Table 4) that prevented points on a muscle from moving past a specified geometric boundary represented by a 3-D object (Van der Helm et al. 1992; Delp and Loan 2000). The 3-D objects used were mainly cylinders that prevented movement past the positive (cranial) or negative (caudal) surface of the cylinder. Appendix 4 explains the procedure for defining wrapping surfaces for each muscle (type, 3-D dimensions, and 3-D position), Table 4 provides the final wrapping surface parameters (shape, size, and location) for each muscle, and Figure 3 provides a visualization of the musculoskeletal model.

Muscle Moment Arm Calculation.—The musculoskeletal model uses the ''partial velocity'' method (Delp and Loan 1995) to calculate moment arms as a function of joint angle. First, we investigated the relationship between muscle moment arms and joint angles, using our initial ''best guess'' assumptions about joint axes, muscle attachments, and three-dimensional paths (including wrapping surfaces and via points). Although the moment arms for some muscles about particular joints changed slightly if we altered the angles at other joints (e.g., the hip extensor moment arm varied slightly with knee flexion for some muscles), these changes were usually small and are not a focus of this study. Thus all flexion/extension limb joint angles except the one of interest (hip, knee, ankle, or toe joint flexion/extension) were kept in the fully columnar pose (0°) while we examined how muscle moment arms changed with the joint angle for one joint. Moment arms for flexion/extension were computed about the mediolateral axis of each joint (which typically was close to the global z-axis).

Second, we systematically varied model parameters (origins, insertions, and path constraints such as wrapping surfaces) to see how much errors in these assumed parameters affected our conclusions. In particular, we fo-
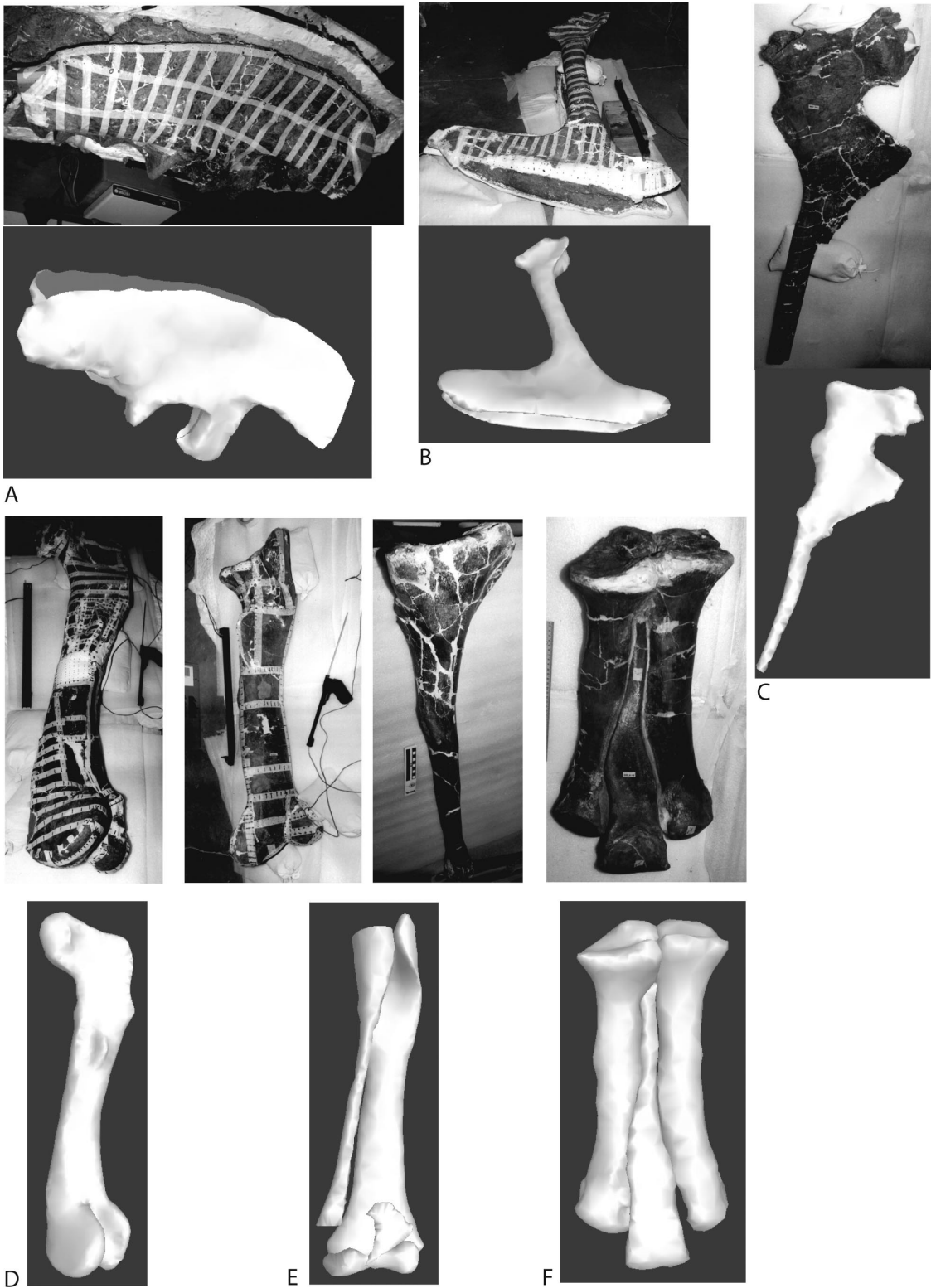
FIGURE 1.   Original fossil bones (above) and 3-D computer bone image files (below) of *Tyrannosaurus rex*, from Museum of the Rockies specimen MOR 555. A, Right ilium in dorsolateral view. B, Pubes in right ventrolateral view. C, Right ischium in lateral view. D, Right femur in oblique caudomedial view. E, Right tibia (on left, cranial view)

cused on those muscles for which we know the least about origin or insertion (including size) and three-dimensional paths in *Tyrannosaurus*, choosing four muscle groups to analyze for the ''worst case'' effects of our assumptions. The location of the iliac origin and the geometry of the knee extensor wrapping surface for M. iliotibialis 3 (IT3) are uncertain and perhaps crucial for the function of this extensor of the hip and knee joints, so we varied these parameters (moving the origin cranially or caudally 0.10 m, and increasing or decreasing the wrapping surface radius by 25%; these numbers are subjective estimates of possible error). Moving the M. iliotibialis 3 origin cranially required a 0.10 m craniad translation of the hip joint wrapping cylinder as well. For M. iliotrochantericus caudalis (ITCA, ITCP) and M. iliofibularis (ILFB), the relative sizes of these muscles are contentious (e.g., Romer 1923; Walker 1977) and muscle scars offer little clarity regarding their precise positions, so we varied the iliac origins by ±0.10 m cranially/caudally. When we moved the M. iliofibularis origin caudally by 0.10 m, we had to increase its hip joint wrapping surface by 0.10 m radius as well to constrain its path. Likewise, we adjusted the hip joint wrapping cylinder for the ITCA (the ITCP had none) by increasing (for the cranially displaced origin) or decreasing (for the caudally displaced origin) its radius by 33%. For M. iliotrochantericus caudalis and M. iliofibularis, we also did a preliminary investigation of the effects of these changes on moment arms in three dimensions, visualizing joint angle changes for long-axis rotation moment arms (ITCA, ITCP) and for abduction moment arms (ILFB) about the hip. Finally, we noticed that our assumptions about how to model the geometry of the ankle wrapping surface were crucial for estimating the moment arms of the ''Achilles tendon'' and other muscle groups, so we varied the wrapping surface for M. gastrocnemius lateralis (GL) by (1 and 2) rotating it 10° about the y-axis medially and then laterally; (3) increasing its radius 33% (to 0.20 m), and (4) translating its location 0.06 m distally to align with the ankle joint flexion/extension axis rather than with the bony condyle morphology.

Model Results

Results.—Hip flexor and extensor moment arms for *Tyrannosaurus* varied substantially with flexion and extension of the hip joint (Fig. 4). Some muscles varied more than others, although the maximum values for many muscles were two or more times the minimum values (Table 5), especially ''hamstrings'' such as M. flexor tibialis internus (FTI1, FTI3) or the adductors (ADD1, ADD2). As expected, muscles that followed wrapping surfaces for all or most of their range of motion had less variation than muscles without wrapping surfaces. An important trend we observed is a decrease of extensor muscle moment arms with increasing joint flexion (e.g., Biewener 1989, 1990; Buford et al. 1997; Maganaris 2004). Key hip extensors such as M. iliotibialis 3 (IT3), M. iliofibularis (ILFB), M. flexor tibialis externus (FTE), and M. caudofemoralis longus (CFL) exhibited noteworthy increases (15–28% change from minimum to maximum values) of their extensor moment arms with hip joint extension (Fig. 4A–D), paralleling a similar trend for the lower limb extensor muscle moment arms and joint angles (Fig. 5). As the latter muscles were likely the largest hip extensors, overall capability to produce hip extensor moments should have declined with hip flexion beyond a fairly upright pose (Fig. 6). One exception (Fig. 4A) to this trend was M. ambiens (AMB), which had a hip extensor moment arm that increased with hip flexion, switching from having an extensor moment about the hip to a flexor moment at about −30° of flexion (from the columnar reference pose with the femur at a 90° angle to the pelvis). Likewise, M. ischiotrochantericus (ISTR) and M. puboischiofemoralis internus 3 (PIFE3)

←

and left fibula (on right, lateral view; reversed in model to be right element; original astragalus and calcaneum not shown), combined into a ''tibiotarsus'' in cranial view, below (the absence of the calcaneum, distal fibula, and part of the astragalus does not affect our model results appreciably). F, Right metatarsals II–IV in cranial view. Parts of the digitizing apparatus are also shown in A–E. Images are not to scale.
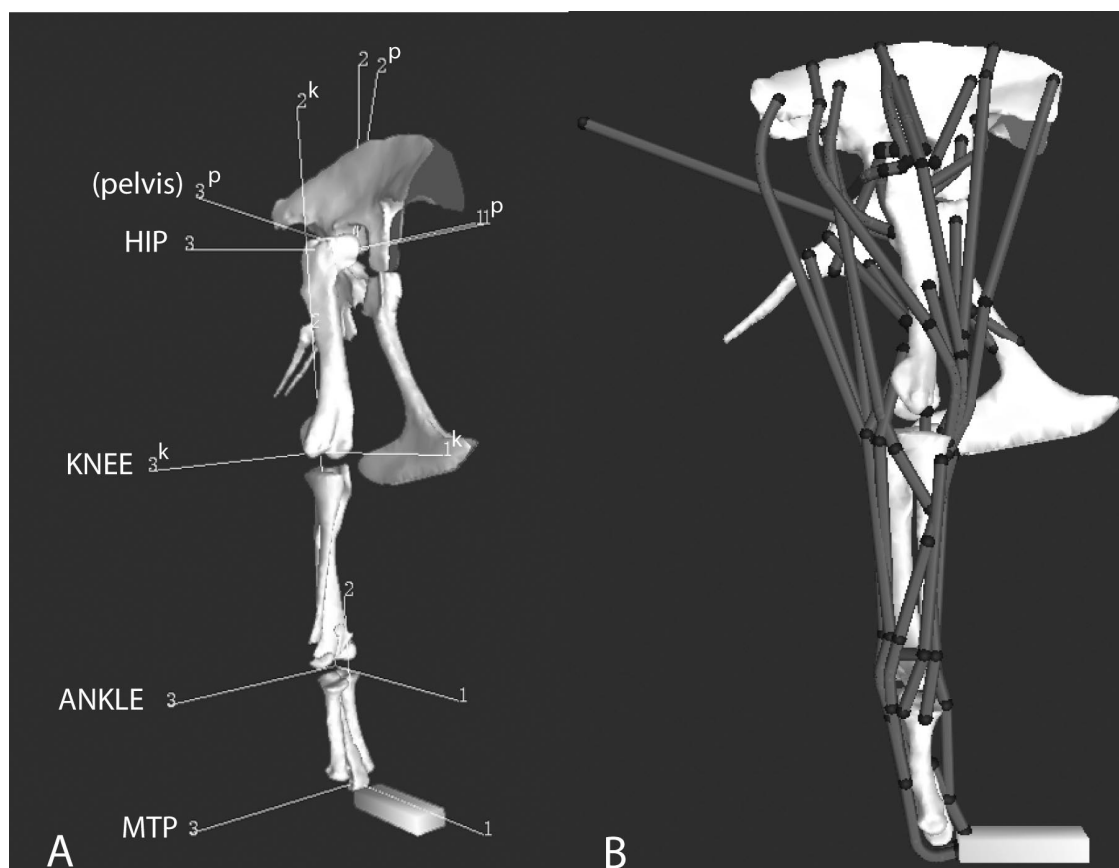
FIGURE 2. Initial musculoskeletal model of *Tyrannosaurus rex*. A, Joint axis definitions for the 3-D model, in oblique craniolateral view (also see Table 1). The x, y, and z-axes are labeled 1, 2, and 3 respectively for each joint defined in the model; "(pelvis)" represents the pelvis segment origin and "MTP" is the toe joint (which used modified axes; Appendix 2). The pelvis and knee axes are marked with "p" and "k" superscripts to identify them more clearly. Furthermore, the space added between the joint centers to accommodate for soft tissues (Appendix 2) displaces the axes along the y-axis (proximodistally), so they do not lie where one might expect them to be anatomically (e.g., the ankle axis appears to float in empty space). The hip and "pelvis" z-axes (labeled 3) appear offset from each other because of the knee valgus angle adopted (see Appendix 2). The y-axis (labeled 2) of the knee joint is elongated here so that it can be seen (above the hip joint); the same axis for the ankle is mostly hidden inside the tibial bone segment. For all joints, the muscle moment arms in flexion-extension were calculated about the z-axis (labeled 3). Hip joint adduction-abduction and knee varus-valgus were about the x-axis (labeled 1), whereas hip medial-lateral rotation was about the y-axis (labeled 2). B, Lateral view of all 37 muscle groups incorporated in the model. Figure 3 shows these in more detail; also see Tables 2, 3. For simplicity only the right leg is shown in all figures, but the model has a left leg that is a mirror image of the right and can optionally be visualized as well.

showed increased hip extensor moment arms with hip flexion (Fig. 4C,D). The latter muscle and M. adductor femoris (ADD1) switched from hip extensor to hip flexor function at about 20° of hip extension (Fig. 4C), as did M. iliofemoralis externus (IFE) and M. puboischiofemoralis internus 3 (PIFE3) at about −30° of hip flexion (Fig. 4B,D). However, some muscles, such as the caudally positioned "hamstrings" (FTI1, FTI3), and adductors (ADD1, ADD2) had peak moment arm values at fairly

extended hip joint angles, around only −5° to −30° of hip flexion (Fig. 4C). Most deep dorsal thigh muscles (ITCA, ITCP, PIFI1, PIFI2) and the pubic heads of M. puboischiofemoralis internus (PIFE1, PIFE2) generally maintained small hip flexor moment arms (Fig. 4B), whereas the largest hip flexor moment arms were for M. iliotibialis 1 and 2A (IT1, IT2A) (Fig. 4A).

For more distal joints, the trend of increasing extensor moment arms with joint exten-

TABLE 1. Ranges of joint motion allowed in the *Tyrannosaurus rex* musculoskeletal model. Asterisk indicates that inclusion of the interphalangeal joint is optional (see Appendix 2). To convert these angles to the angles used in Hutchinson and Garcia 2002; also Hutchinson 2004 a,b, for the hip joint subtract 90° from the angle here, for the knee subtract the angle here from 180°, for the ankle add 180° to the angle here, and for the toe add 90° to our metatarsophalangeal joint angle. For all joints, 0° was fully straightened, so the columnar reference pose has all joint angles set at 0°.

Joint	Motion	Minimum joint angle (°)	Maximum joint angle (°)
Hip	Flexion/extension	−65	45
Hip	Abduction	0	45
Hip	Medial/lateral rotation	−30	30
Knee	Extension/flexion	−10	90
Ankle	Flexion/extension	−90	0
Metatarsophalangeal (Toe)	Flexion/extension	−45	90
Interphalangeal*	Flexion/extension	−45	0
Foot-ground	Medial/lateral rotation	−45	45

sion was more consistent (Fig. 5). Knee extensors all followed this pattern, increasing by up to 170% from strong flexion to extension (Fig. 5A). However, we found more complexity for knee flexor muscle moment arms: although their values tended to decrease in magnitude, from flexor toward extensor moment arms, the ''hamstring'' muscle moment arms also had some of their lowest flexor magnitudes at very flexed knee joint angles (Fig. 5B).

Nonetheless, for the ankle extensor muscles, extensor moment arms increased with joint extension by a factor of about 50% (Fig. 5C). Again, ankle flexor muscles showed more complexity (Fig. 5D): Mm. fibulares longus et brevis (FL, FB) had less extreme ankle flexor moment arms with increased ankle extension, whereas M. tibialis anterior (TA), M. extensor digitorum longus (EDL), and M. extensor hallucis longus (EHL) had their lowest ankle flexor moment arms at very flexed ankle joint angles. The latter pattern was similar to the convexity of the moment arm versus joint angle curves in Figure 5B. However, these muscles presumably were not important for body support in typical poses for *Tyrannosaurus*, which would have required muscles to produce ankle extensor, not flexor, moments to support the limb (Hutchinson and Garcia 2002; Hutchinson 2004b) as in other animals (e.g., Biewener 1989, 1990).

Toe (plantar) flexor moment arms for supporting the metatarsophalangeal joint (important during limb contact with the ground [Hutchinson and Garcia 2002]) remained

around 0.10 m, whereas the toe extensor (dorsiflexor) moment arms varied more, peaking at about 0.13 m at extreme joint extension (−25° dorsiflexion from the reference pose; Fig. 2) and decreasing to about 0.03 m at extreme joint flexion (90° plantarflexion). Because the toe joint flexor and extensor muscles were constrained to wrap around cylindrical surfaces at the digits, their moment arms varied little with toe joint angles, and so are not plotted. This is expected, as muscle-tendon units that are constrained to wrap tightly around cylinders should have constant moment arms equal to the radius of the cylinders, if those cylinders are aligned to the joint axis.

Sensitivity Analysis of Unknowns.—The moment arms of key pelvic and thigh muscles in *Tyrannosaurus* should vary with the assumptions made for their three-dimensional paths, including origins and insertions. We infer that some pelvic muscles (Fig. 3: AMB, ADD1, ISTR, and CFB) have reasonably certain attachment points proximally and distally because of clear osteological correlates (Carrano and Hutchinson 2002). Hence we are confident in their paths and moment arms. This confidence also extends to other muscles (e.g., Mm. femorotibiales or most lower limb muscles) whose exact centroids of origin are uncertain because they have wide fleshy origins, but whose moment arms (e.g., about the knee, or the ankle or toes for most lower limb muscles) are more certain because their paths are clearly defined by osteological landmarks such as the extensor groove of the distal femur

TABLE 2. Pelvic and thigh muscles included in the *Tyrannosaurus rex* musculoskeletal model. For details on the methods and evidence used for these 22 main groups, see Carrano and Hutchinson 2002.

Muscle	Abbreviation	Origin	Insertion
Triceps femoris group:			
M. iliotibialis 1	IT1	Craniodorsal rim of lateral ilium: scar	Tibial cnemial crest
M. iliotibialis 2 (anterior and posterior parts)	IT2A, IT2P	Dorsal rim of preacetabular ilium: roughening	Tibial cnemial crest
M. iliotibialis 3	IT3	Dorsal rim of postacetabular ilium: roughening	Tibial cnemial crest
M. ambiens	AMB	Pubic tubercle	Tibial cnemial crest; and secondary tendon to join FDL
M. femorotibialis externus	FMTE	Lateral femoral shaft: smooth region between intermuscular lines	Tibial cnemial crest
M. femorotibialis internus	FMTI	Craniomedial femoral shaft: smooth region between intermuscular lines	Tibial cnemial crest
M. iliofibularis	ILFB	Lateral postacetabular ilium between IFE and FTE	Fibular tubercle: scar
Deep dorsal group:			
M. iliofemoralis externus	IFE	Lateral ilium: no clear scar	Femoral trochanteric shelf: scar
M. iliotrochantericus caudalis (anterior and posterior parts)	ITCA, ITCP	Lateral preacetabular ilium: no clear scars	Femoral lesser trochanter (ITCA distal to ITCP)
M. puboischiofemoralis internus 1	PIFI1	Iliac preacetabular fossa: no clear scar but cranial to PIFI2	Craniomedial proximal femur: scar
M. puboischiofemoralis internus 2	PIFI2	Near iliac preacetabular fossa (position is equivocal)	Femoral accessory trochanter
Flexor cruris group:			
M. flexor tibialis internus 1	FTI1	Ischial shaft: tubercle	Medial proximal tibia: no clear scar
M. flexor tibialis internus 3	FTI3	Ischial tuberosity: scar	Medial proximal tibia: no clear scar
M. flexor tibialis externus	FTE	Lateral postacetabular ilium: scar	Medial proximal tibia: no clear scar
Adductors:			
M. adductor femoris 1	ADD1	Cranioventral edge of ischial obturator process	Caudomedial distal femoral shaft: scar
M. adductor femoris 2	ADD2	Caudodorsal rim of ischium: scar/groove	Caudomedial distal femoral shaft: scar
Mm. puboischiofemorales externi:			
M. puboischiofemoralis externus 1	PIFE1	Cranial surface of pubic apron: no clear scar	Femoral greater trochanter
M. puboischiofemoralis externus 2	PIFE2	Caudal surface of pubic apron: no clear scar	Femoral greater trochanter
M. puboischiofemoralis externus 3	PIFE3	Lateral surface of obturator process, between ADD1+2: no clear scar	Femoral greater trochanter
M. ischiotrochantericus	ISTR	Medial surface of ischium: no clear scar	Femoral trochanteric shelf: scar
Mm. caudofemorales:			
M. caudofemoralis brevis	CFB	Iliac brevis fossa	Lateral surface of fourth trochanter
M. caudofemoralis longus	CFL	Caudal vertebral centra 1–15	Medial surface of fourth trochanter: scar

TABLE 3. Lower limb muscles included in the *Tyrannosaurus rex* musculoskeletal model. For details on the methods and evidence used for these 11 muscle groups, see Carrano and Hutchinson 2002.

Muscle	Abbreviation	Origin	Insertion
Mm. gastrocnemii:			
M. gastrocnemius lateralis	GL	Caudal surface of distal femur: scar	Caudal surfaces of metatarsals II–IV: scars
M. gastrocnemius medialis	GM	Medial proximal tibia: no clear scar	With GL
Digital flexors:			
M. flexor digitorum longus	FDL	Focused on area near GL origin: no clear scar	Ventral pedal phalanges II–IV: flexor tubercles
M. flexor digitorum brevis	FDB	Caudal surface of metatarsals II–IV: no clear scar	Ventral pedal phalanges II–IV: flexor tubercles
M. flexor hallucis longus	FHL	With GL and FDL origins	Ventral pedal phalanx I: flexor tubercle (medial side of metatarsus)
Digital extensors:			
M. extensor digitorum longus	EDL	Craniomedial surface of proximal femur/tibia: no clear scar	Dorsal pedal phalanges II–IV: no clear scars
M. extensor digitorum brevis	EDB	Cranial surface of metatarsals II–IV: no clear scar	Dorsal pedal phalanges II–IV: no clear scars
M. extensor hallucis longus	EHL	Distal fibula: no clear scar	Dorsal pedal phalanx I: no clear scar (cranial side of metatarsus)
M. tibialis anterior	TA	Cranial surface of proximal tibia: no clear scar	Cranial proximal metatarsals II–IV: scar and tubercle
Mm. fibulares:			
M. fibularis longus	FL	Craniolateral fibular and tibial shafts: no clear scar	Caudolateral proximal metatarsals II–IV: no clear scar; and secondary tendon to FDL
M. fibularis brevis	FB	Distal to FL on fibula: no clear scar	Craniolateral proximal metatarsals II–IV: no clear scar

(Hutchinson 2001b), tibial crest (Carrano and Hutchinson 2002; Hutchinson 2002), or other areas for tendon passage (e.g., distal tibia, proximal metatarsus, and flexor tubercles of the phalanges for the lower limb muscles).

Nonetheless, as shown in Figure 7, the assumed centroids of origin for some muscles, varied within reasonable bounds, do make a considerable difference for the moment arms calculated about some joints, particularly the hip joint. For example, repositioning the M. iliotibialis 3 (IT3) centroid of origin 0.10 m cranially or caudally changes its hip extensor moment arm by almost the same amount, and changes how its moment arm changes with hip joint flexion (Fig. 7A). Recall that the IT3 wrapping surface was moved in the case of cranially repositioning the origin, but it was not moved for the caudally repositioned origin. Given that the scar for the origin of this

muscle does not unambiguously indicate where the centroid was, future studies need to consider how much the moment arm of this muscle might vary and the influence of that variation on the results of any biomechanical analysis. Similarly, the knee extensor moment arm of the same muscle (and all knee extensors) depends on the size of the wrapping surface (Fig. 7A); a 25% change of wrapping surface radius can change the moment arm by 25%. In this study, we rather arbitrarily used the sizes of osteological features along the muscle path (Appendix 2) to gauge the initial radius size, although it is hard to conceive that it was much larger (see Fig. 8). Our model has the advantage that we did not consider muscles in isolation—the relative positions of muscles with respect to each other were accounted for in our initial assumptions about muscle paths and wrapping surfaces, to pre-

TABLE 4. Wrapping surfaces placed in the *Tyrannosaurus rex* musculoskeletal model: cylinders (top rows) and ellipsoids (bottom rows). The ''Muscle'' column indicates the muscle symbol (see Table 2). The ''Location'' column shows where the wrapping object was attached. The ''r'' columns note the rotations (in degrees) of the wrapping objects about the x, y, and z segment axes. The ''t'' columns list the translations (in meters) of those objects from the segment origins. The ''Radius'' and ''Height'' columns give object dimensions (in meters). An asterisk indicates that the pubic shaft wrapping surface was also used for Mm. flexores tibiales internus 1 (FTI1) et externus (FTE) in extreme joint positions.

Muscle	Location	Shape	r(x)	r(y)	r(z)	t(x)	t(y)	t(z)	Radius	Height
IT2A	Middle of lateral ilium	cylinder	0	90	0	0.54	0.05	0.00	0.32	2.00
IT2P	Femoral shaft	cylinder	0	90	0	0.07	0.02	−0.05	0.30	2.00
IT3	Postacetabular ilium	cylinder	−10	10	0	−0.10	0.00	0.02	0.40	1.00
ILFB	Postacetabular ilium	cylinder	−10	30	0	0.00	0.00	0.05	0.40	0.50
ITCA	Preacetabular ilium	cylinder	10	0	0	0.10	0.29	0.00	0.15	1.00
PIFI1	Postacetabular ilium	cylinder	0	0	0	0.19	0.00	0.00	0.05	0.50
PIFI2	Postacetabular ilium	cylinder	0	0	0	0.25	0.10	0.00	0.10	0.50
FTE	Postacetabular ilium	cylinder	0	10	0	−0.20	0.00	0.20	0.50	0.75
PIFE1+2	Femoral shaft	cylinder	95	0	0	0.01	−0.60	0.12	0.15	1.20
CFB	Postacetabular ilium	cylinder	10	10	0	−0.11	−0.10	−0.07	0.25	1.00
CFL	Femoral shaft	cylinder	0	10	0	−0.07	−0.05	0.00	0.35	1.00

									Radius	Radius	Radius
Muscle	Location	Shape	r(x)	r(y)	r(z)	t(x)	t(y)	t(z)	(x)	(y)	(z)
IT1	Craniolateral ilium	ellipsoid	−25	−15	−10	0.72	0.30	0.01	0.50	0.20	0.06
IT1	Preacetabular ilium	ellipsoid	0	0	0	0.02	0.00	−0.50	0.50	0.50	1.00
IFE	Dorsolateral proximal femur	ellipsoid	−10	0	0	0.00	0.12	0.10	0.20	0.30	0.20
FTI3	Ventral pelvis	ellipsoid	10	10	−45	0.09	−0.36	0.10	0.60	0.15	0.10
ADD1+2*	Pubic shaft	ellipsoid	0	0	30	0.36	−0.73	−0.02	0.08	0.70	0.10
ISTR	Femoral shaft	ellipsoid	0	−25	0	−0.11	−0.10	0.06	0.08	0.25	0.20

vent muscles from entering space that was likely occupied by other muscles. Additionally, most muscles (except Mm. caudofemorales) probably did not extend far from the craniocaudal ends of the pelvis, as in living animals. Larger wrapping surfaces would probably violate these constraints.

For M. iliotrochantericus caudalis, we split this muscle into two parts (ITCA and ITCP), and investigated the effect of positional variation of these muscle origins on hip moment arms (Fig. 7B). Because these muscles traveled at oblique lines of action to the hip joint, error in placing their origins was not as problematic as for M. iliotibialis 3; a 0.10 m cranial/caudal change of position had up to a ±0.02 m effect on hip flexor moment arms and a ±0.05 m effect on medial rotation moment arms. The function of the ITCP part, however, depended strongly on where the origin was placed: in a slightly more cranial position, it switched from a very weak lateral rotator to a weak medial rotator of the hip, whereas the ITCA part

only changed the relative magnitude of its moment arm. Thus muscles whose inferred lines of action pass close to the hip joint (and hence might switch their moment arms from flexion to extension or otherwise) deserve careful focus.

Like M. iliotibialis 3, the hip extensor moment arms of M. iliofibularis were strongly influenced by assumptions about exact positioning of the origin centroid and wrapping surface size (Fig. 7C). However, the magnitude of this influence depended on the hip joint angle assumed, becoming more extreme at more extended hip joint angles (up to ± almost 0.10 m with a caudal/cranial shift) whereas at low degrees of hip flexion having little influence ±0.01 m). A 25% increase of the hip joint wrapping surface radius increased the hip extensor moment arm by over 25%, moreso if the origin was shifted 0.10 m caudally as well. Furthermore, when hip abduction moment arms were examined, the effects of path geometry were complex: abduction moment

arms decreased with a caudal shift of the origin but increased with a larger wrapping surface, yet this influence was most marked (± less than 0.05 m) at intermediate joint angles. Thus assumptions about the paths of muscles in extinct taxa can be more or less influential on muscle mechanics depending on the orientation of joints that the muscles cross.

Although the path of M. gastrocnemius lateralis across the ankle joint is fairly clear with respect to the y-axis of the tibia segment (i.e., roughly parallel to it), it is not clear how far caudally its tendon might have passed behind the ankle joint, and this distance determines the extensor moment arm (Fig. 7D). We originally positioned a cylindrical wrapping surface to align with the condyles of the astragalus. Rotating this cylinder ±10° laterally/ medially changed the slope of the moment arm versus joint angle curve slightly, having negligible effect on moment arms at flexed ankle joint positions, but a ±0.01 m influence at extended joint positions. The wrapping surface geometry had more effects on the ankle extensor moment arm when the radius was enlarged 33%, although this influence was not linear, reaching a minimum change of +18% at a fully extended joint angle (0°) and a maximum change of +65% at a fully flexed joint angle (−90°). Shifting the position of the wrapping cylinder to align with the exact position of the ankle joint axis (including empty space added for soft tissues), not the bony contours, made the ankle moment arm constant at 0.15 m (= wrapping surface radius) at all joint angles, not increasing with ankle extension as in our initial model. This is not a surprising result as it should apply to any joint given a large wrapping surface aligned to the joint axis, but experimental data show that such situations are extremely unusual in living animals (e.g., Spoor and Van Leeuwen 1992; Buford et al. 1997; Delp et al. 1999; Pandy 1999; Thorpe et al. 1999; Arnold et al. 2000; Arnold and Delp 2001; Kargo and Rome 2002; Brown et al. 2003a,b; Krevolin et al. 2004; Maganaris 2004). Thus although some assumptions (e.g., the rotation of wrapping cylinders) may have small effects, other effects may be nonlinear or may obliterate trends (such as increasing extensor moment arms with in-

creased joint extension) that are pronounced when using other assumptions. In these somewhat ''worst case'' situations, we expect maximum errors in our model of around ±25%, or ±65% in very extreme cases. These errors are comparable to the largest errors in other methods (e.g., Arnold et al. 2000; Brown et al. 2003a,b; Maganaris 2004), although we should caution that they are merely our ''best guesses'' at possible errors. Nonetheless, barring exceptional soft tissue preservation, it is unlikely much better ''guesses'' can be made. In any case, the benefit of our model is that any potential error can be quantitatively assessed, whereas without such a model it is likely that complexities in musculoskeletal geometry (well represented in our model) would be overlooked. Overall, our sensitivity analysis gives us confidence that our general conclusions (see ''Discussion'') will hold even though specific quantitative conclusions depend on the muscle path-related assumptions and could involve substantial error.

Discussion

We begin by discussing the broader implications of our study for understanding how muscle moment arms change with body size, by considering the muscle moment arms of *Tyrannosaurus rex* in comparison with other animals. We also evaluate how the moment arm values we calculated compare with assessments of dinosaur hindlimb muscle function in other studies. Next, we integrate our model results with other data to reconstruct aspects of locomotor function (stance, gait, and speed) in *T. rex*. Finally, we consider how this simple musculoskeletal model can be improved and expanded in future studies.

Muscle Moment Arms: Size-based Comparisons.—The large pelvis of *Tyrannosaurus rex* should have placed the hip muscles at large distances from the hip joint, providing them with large moment arms, much as in birds (Tables 5, 6, Figs. 4, 6) (Hutchinson 2004a,b: Table 6). Were the extensor muscle moment arms of *T. rex* larger than one would expect for its size, as expected if allometric patterns in smaller animals could be maintained to such large sizes (Maloiy et al. 1979; Alexander et al. 1981; Biewener 1989, 1990; Hutchinson
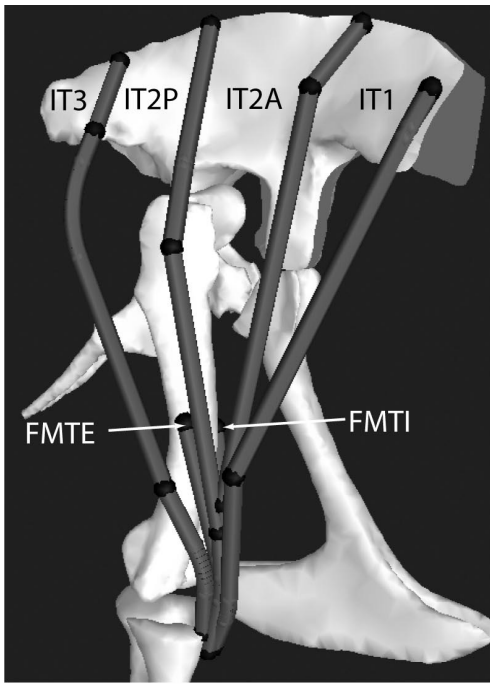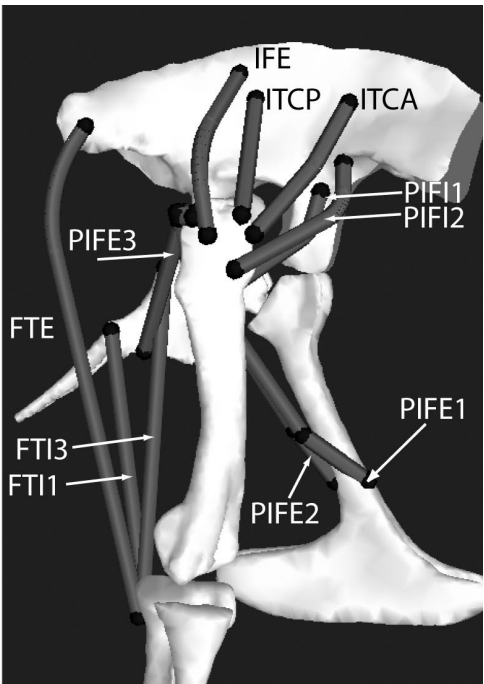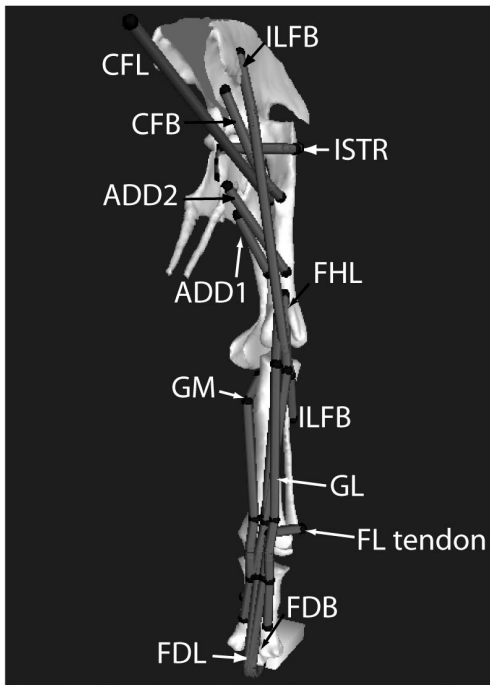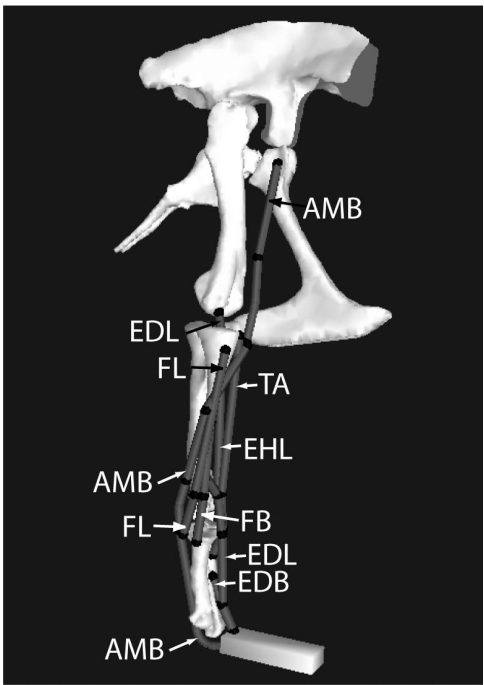
2004b)? Strong allometry of muscle leverage ($\sim$body mass$^{0.4}$) is crucial for maintaining high level locomotor performance as size increases (Maloiy et al. 1979; Alexander et al. 1981; Biewener 1989, 1990; Bennett and Taylor 1995), yet such allometry is clearly lacking (instead being closer to isometry; also see Hutchinson 2004b) for most muscles and joints in *T. rex* (Table 6, Fig. 8). Unfortunately, comparative scaling data for hip extensor muscle moment arms in extant taxa are almost nonexistent, presumably because without a 3-D model hip moment arms are harder to accurately measure than moment arms for more distal muscles.

Scaling from published data for birds and mammals (Table 6) to a 6000 kg body mass (a reasonable estimate of the mass of MOR 555 [Farlow et al. 1995]) predicts moment arm values for most extensor muscles distal to the hip joint that are 40–600% higher than this study shows for *Tyrannosaurus rex*. For example, for our initial model of *T. rex* we obtain knee extensor moment arms of 0.17–0.23 m in the reference pose (average 0.20 m), less with more flexed knees (Fig. 5A). Scaling equations for extant animals show that the average knee extensor moment arm for *T. rex* is unexceptional for a quadruped and is smaller than expected for a running biped. This observation is even more strongly pronounced for the ankle joint of *T. rex* (moment arm less than 0.13 m in all poses; Fig. 5C), and a similar pattern holds for the few data available for toe plantarflexor moment arms (Table 6). These findings include reasonable considerations of soft-tissue effects on wrapping surfaces and hence moment arms, so we see no way that the distal limb extensor moment arms of *T. rex* could have been apomorphically or allometrically large. This runs in stark contrast to some intuitive studies of tyrannosaur leg muscle functional

anatomy, which have suggested that tyrannosaurs had unusually great muscle leverage (e.g., Bakker 1986, 2002; Paul 1988, 1998; Leahy 2002). The reason these studies came to such conclusions appears to be the large (to human eyes) sizes of muscle attachment sites and bony prominences such as the cnemial crest of the tibia (Fig. 8) or ''hypotarsus'' of the proximal metatarsus (also see Molnar and Farlow 1990; Hutchinson 2004b). If tyrannosaurs had extensor muscles with high effective mechanical advantage for their size (i.e., moment arm allometry $\sim$ body mass$^{0.4}$), their moment arms should have been roughly twice or more as large as most of those estimated in this study (Table 6, Fig. 8); even more so if the body mass of an adult *T. rex* was more than 6000 kg, as some studies suggest (e.g., Henderson 1999). This presents another problem for reconstructions of large theropods moving at high speeds, discussed more below. Our sensitivity analysis shows us that this conclusion would not be reversed by applying reasonable alternative muscle reconstructions; there is no realistic way to grant the hindlimb extensor muscles of *T. rex* the high effective mechanical advantage that some studies have implied it had.

Comparison with Other Studies of Dinosaur Hip Muscle Function.—Although much attention has been given to changes in archosaurian hip muscle function with evolutionary changes in anatomy and limb orientation (e.g., Romer 1923; Colbert 1964; Charig 1972; Russell 1972; Walker 1977; Perle 1985; Gatesy 1990; Carrano 2000; Hutchinson and Gatesy 2000), there has been little focus on how muscle function in an individual animal depended on its limb orientation, as we have done here. Walker (1977) did discuss how flexor moment arms of M. puboischiofemoralis internus (PIFI) would have decreased in dinosaurs as the hip joint was

←

FIGURE 3. Muscle groups included in the musculoskeletal model of the right hindlimb of *Tyrannosaurus rex*, in the reference pose with initial muscle attachments used. See Table 2 for muscle abbreviations. A, ''Triceps femoris'' knee extensor muscles (except AMB), in craniolateral view. B, Deep dorsal (IFE, ITCA, ITCP, PIFI1, and PIFI2), Mm. puboischiofemorales externi (PIFE1–3), and ''hamstring'' (FTI1, FTI3, FTE) thigh muscles, in lateral view. C, Other caudally positioned pelvic muscles, and lower leg muscles on the plantar (caudal) surface of the limb, in caudal view. M. flexor digitorum brevis (FDB) is partly hidden underneath the FDL, and the secondary tendon of M. fibularis longus (FL) is shown crossing laterally to join the digital flexors. D, M. ambiens (AMB) and lower leg muscles on the dorsal (cranial) surface of the limb, in craniolateral view.
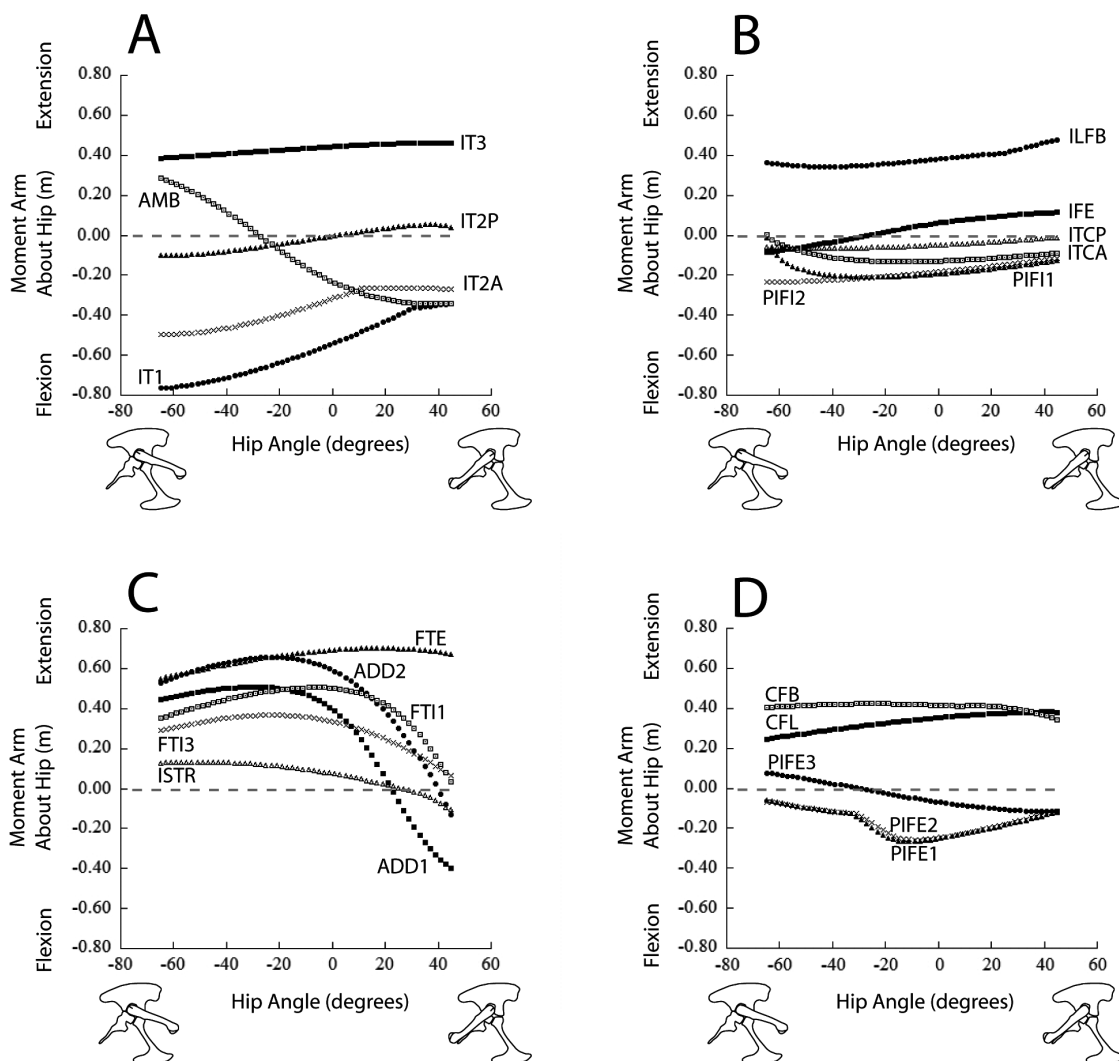
FIGURE 4. Changes in hip extensor muscle moment arms plotted against hip joint flexion/extension angle for *Tyrannosaurus rex*. Negative angles and moment arms are for hip flexion (from the straight-limbed reference pose); positive angles and moment arms are for hip extension (toward the right on the x-axis). A, M. iliotibialis 1–3 (IT1–3) and M. ambiens (AMB). B, M. iliofibularis (ILFB), M. iliofemoralis externus (IFE), M. iliotrochantericus caudalis (ITCA, ITCP), and Mm. puboischiofemoralis internus 1+2 (PIFI1+2). C, Mm. flexores tibiales interni 1 et 3 (FTI1, FTI3) et externus (FTE), Mm. adductores femorii 1+2 (ADD1, ADD2), and M. ischiotrochantericus (ISTR). D, Mm. puboischiofemorales externi 1–3 (PIFE1–3) and Mm. caudofemorales brevis et longus (CFB, CFL). Only those muscles that had non-zero values for moment arms are shown. For simplicity, here we focus on the sagittal plane (flexion/extension) action of muscles, although the hip joint allowed muscles to incur abduction and long-axis rotation as well, which we comment on briefly in the Discussion (and Fig. 7).

flexed during femoral protraction, but switches in function from flexion to extension or vice versa to our knowledge have not been seriously contemplated. For example, the M. iliotibialis 2 postacetabular part (IT2P) moment arm about the hip varied from flexor to extensor in strongly flexed to extended poses (Fig. 4A), corresponding to a potential change in its

function. We found similar patterns for other muscles, including AMB, IFE, ADD1, and PIFE3 (Fig. 4), which are well-documented for analogous muscles in humans (e.g., Delp et al. 1999). Studies of muscle function in extinct animals such as dinosaurs should be cautious to investigate this possibility for these and other muscles before assuming that muscle func-

TABLE 5. Results for hip joint moment arms of major pelvic muscle groups in *Tyrannosaurus rex*. Muscle names, abbreviations, and moment arms at 0° and 45° hip joint angles, and minimum, maximum, and mean values are presented. All units are in meters; negative moment arms are hip flexor whereas positive are extensor. For muscles acting about other joints, see Figures 5 and 8.

Muscle	Abbr.	At 0°	At 45°	Min	Max	Mean
M. iliotibialis 1	IT1	−0.34	−0.54	−0.77	−0.34	−0.57
M. iliotibialis 2 (preacetabular part)	IT2A	−0.27	−0.32	−0.50	−0.26	−0.37
M. iliotibialis 2 (acetabular part)	IT2P	0.04	0.00	−0.10	0.05	−0.02
M. iliotibialis 3	IT3	0.46	0.44	0.39	0.46	0.43
M. ambiens	AMB	−0.34	−0.23	−0.34	0.28	−0.11
M. iliofibularis	ILFB	0.47	0.38	0.34	0.47	0.38
M. iliofemoralis externus	IFE	0.11	0.06	−0.09	0.11	0.03
M. iliotrochantericus caudalis (anterior part)	ITCA	−0.09	−0.13	−0.13	0.00	−0.11
M. iliotrochantericus caudalis (posterior part)	ITCP	−0.01	−0.05	−0.06	−0.01	−0.05
M. puboischiofemoralis internus 1	PIFI1	−0.11	−0.18	−0.24	−0.11	−0.19
M. puboischiofemoralis internus 2	PIFI2	−0.13	−0.19	−0.21	−0.01	−0.17
M. flexor tibialis internus 1	FTI1	−0.13	0.59	−0.13	0.66	0.49
M. flexor tibialis internus 3	FTI3	0.06	0.34	0.06	0.37	0.29
M. flexor tibialis externus	FTE	0.67	0.69	0.55	0.70	0.66
M. adductor femoris 1	ADD1	−0.40	0.40	−0.40	0.51	0.28
M. adductor femoris 2	ADD2	0.04	0.50	0.04	0.51	0.41
M. puboischiofemoralis externus 1	PIFE1	−0.12	−0.25	−0.27	−0.06	−0.17
M. puboischiofemoralis externus 2	PIFE2	−0.12	−0.25	−0.26	−0.07	−0.17
M. puboischiofemoralis externus 3	PIFE3	−0.12	−0.07	−0.12	0.08	−0.04
M. ischiotrochantericus	ISTR	−0.11	0.08	−0.11	0.13	0.07
M. caudofemoralis brevis	CFB	0.38	0.35	0.25	0.38	0.33
M. caudofemoralis longus	CFL	0.34	0.42	0.34	0.42	0.41

tions are fixed properties, as they are often portrayed.

The tendency for extensor muscle moment arms to increase with joint extension matches similar trends in other studies using tendon excursion (An et al. 1984) or computer modeling (Pandy 1999) methods; e.g., for horses (Brown et al. 2003a,b) and humans (personal manipulations of models from Delp et al. 1990; Buford et al. 1997; Maganaris et al. 2004). In these studies, moment arms tended to reach their maxima near complete joint extension, as in this study (e.g., at around a −15° hip joint angle; Fig. 6). We caution that there are exceptions to this pattern (Fig. 4), but this general conclusion is likely to hold for most extensor muscles. However, we also caution that although we feel that we have made reasonable assumptions about muscle path geometry in our initial model, Figure 7 shows how influential those assumptions can be. In particular, the ankle moment arm versus joint angle pattern relies on our assumptions about wrapping surface geometry. Additionally, muscle force-length (and force-velocity) properties may be more important than moment

arms in determining peak muscle moments about joints (e.g., Brown et al. 2003a,b) and hence more influential in determining optimal joint angles. Our initial results nonetheless pose a problem for reconstructions of *Tyrannosaurus rex* with a ''permanently flexed knee'' (Paul 1988: p. 117) and ''birdlike'' limb function, especially considering the vagaries of anatomical evidence for such pronounced joint flexion (Christiansen 1999; Hutchinson 2004b). The pattern of extensor moment arm decrease with joint flexion (Figs. 4–6) means that more flexed joints have poorer effective mechanical advantage, especially considering that the ground reaction force moment arms opposed by the action of extensor muscles will increase with joint flexion (Biewener 1989, 1990). The ability of those muscles to support the body in their antigravity role would thus be seriously diminished in such poses (Hutchinson and Garcia 2002; Hutchinson 2004b). Hence on biomechanical grounds, because muscular support of body weight would be a challenge for such a large animal, it seems reasonable to reconstruct *T. rex* in a more upright (but not completely columnar) pose, rather
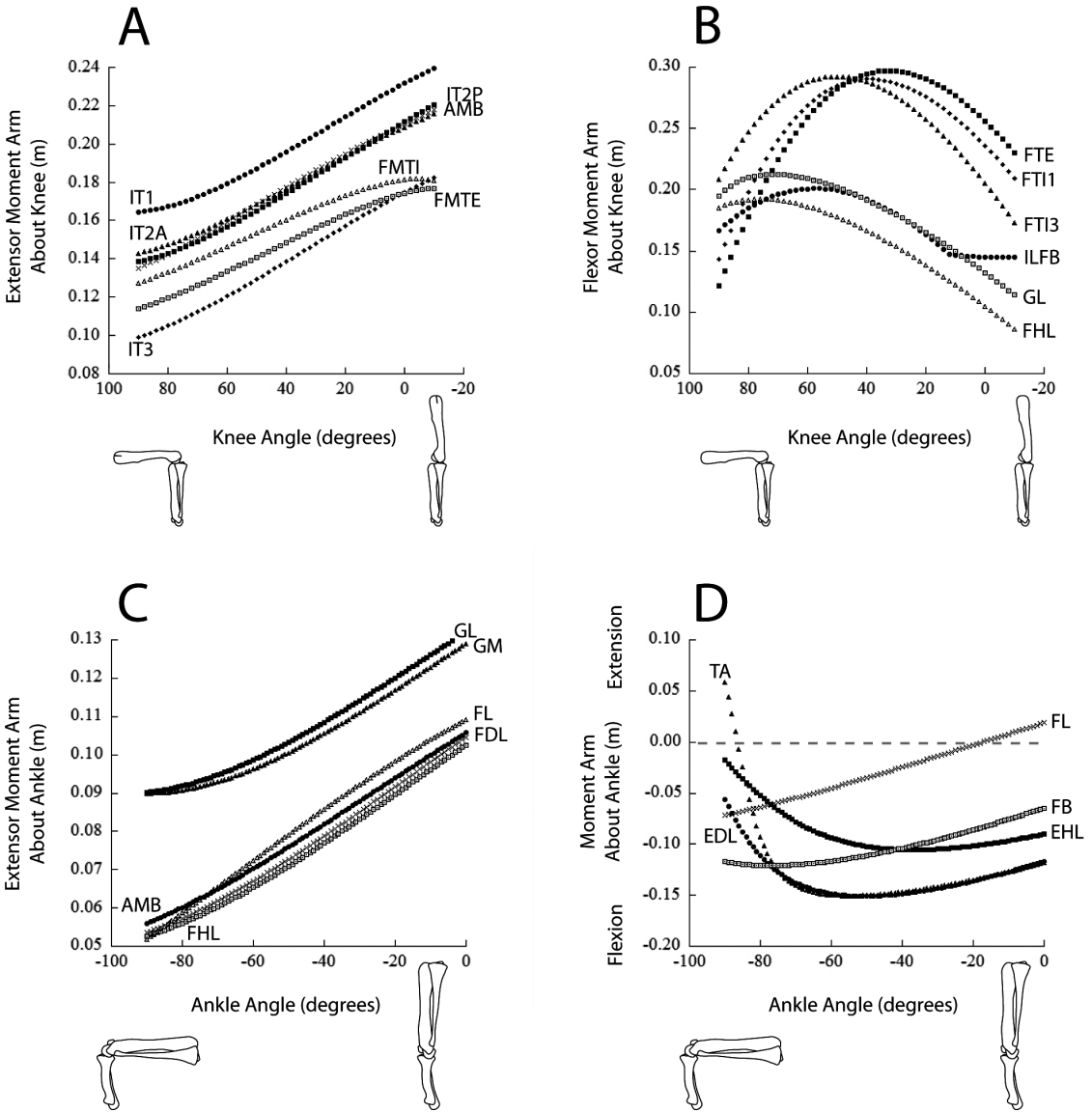
FIGURE 5. Changes in knee (A, B) and ankle (C, D) extensor (A, C) and flexor (B, D) muscle moment arms plotted against knee or ankle joint flexion/extension angle for *Tyrannosaurus rex*. As in Figure 4, more flexed joint angles are toward the left on the x-axis. A, Triceps femoris knee extensor muscles including M. iliotibialis 1–3 (IT1–3), M. ambiens (AMB), and Mm. femorotibiales externus et internus (FMTE, FMTI). B, ''Hamstring'' knee flexor muscles including M. iliofibularus (ILFB), M. flexor tibialis internus 1 and 3 (FTI1, FTI3), and M. flexor tibialis externus (FTE), and the knee flexor moment arms for the ankle extensors M. gastrocnemius lateralis (GL) and M. flexor hallucis longus (FHL). C, Ankle extensor muscles including the GL and FHL as well as M. gastrocnemius medialis (GM), M. flexor digitorum longus (FDL), and the distal secondary tendon of AMB. D, Ankle flexor muscles including M. extensor digitorum longus (EDL), M. extensor hallucis longus (EHL), M. tibialis anterior (TA), and Mm. fibulares longus et brevis (FL, FB). Positive moment arms incur extension, not flexion, in the last graph.

than a more crouched pose (e.g., Lambe 1917; Bakker 1986; Paul 1988, 1998).

Muscles traditionally regarded as important hip flexors, such as M. iliotibialis 1 (IT1) and the preacetabular head of part 2 (IT2A), had large hip flexor moment arms in most

poses (e.g., 0.71 m and 0.37 m respectively; contra Charig 1972). Some authors have considered only a few muscles to have been hip flexors (e.g., M. puboischiofemoralis internus [PIFI] in Perle 1985; also M. puboischiofemoralis externus [PIFE] in Walker 1977), yet it is
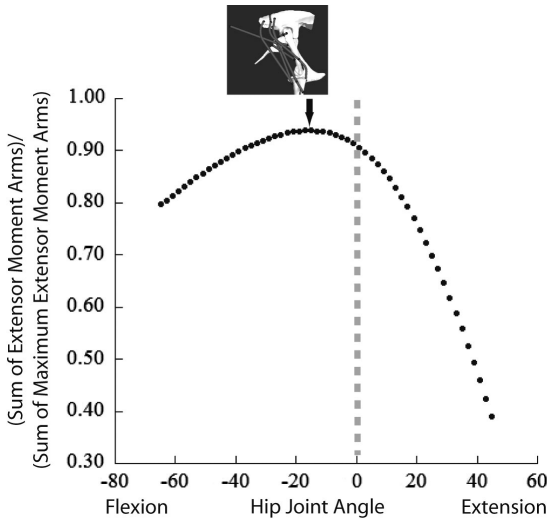
FIGURE 6. Initial results for the hip extensor moment arms of the key hip extensor muscles (IT3, ILFB, FTI1, FTI3, FTE, ADD1, ADD2, ISTR, CFB, and CFL) of *Tyrannosaurus rex* plotted against hip joint angle (as in Fig. 5). The moment arms for all ten muscles have been summed for each hip joint angle, then normalized by the sum of the maximum moment arm value for each muscle (i.e., the peak value for all joint angles). This shows that the hip joint angle (arrow with picture showing muscles and configuration) that optimizes the moment arms of these muscles is quite upright: at about −15° (flexion from the fully columnar reference pose), the moment arms are at about 94% of the peak moment arms; more flexed or extended poses would have had provided relatively less effective muscular support of the body.

clear that many pelvic muscles had hip flexor moment arms (Fig. 4). We do not find, as Walker (1977; also Charig 1972) argued, that the equivalent of his M. iliofemoralis (our two parts of M. iliotrochantericus caudalis; ITCA and ITCP) lacked flexion (protractor) capacity in *Tyrannosaurus rex*, because hip flexor moment arms were as high as −0.15 m (Figs. 4, 7). Moreover, we find no support for Charig's (1972) contention that the expanded ilium (''dolichoiliac'' condition) of dinosaurs such as *T. rex* did not enhance the ability of pelvic muscles to generate hip flexion or extension—it clearly did, as quite a few muscles have larger flexor/extensor moment arms than they would if they were all clustered close to the hip joint, as in basal reptiles. Furthermore, Charig (1972) and others since that classic study have assumed that the range of motion of the femur was restricted to the arc between the pubis and ischium, or at least that the fe-

mur could not be retracted past a line parallel to the ischium (e.g., Paul 1988). As some muscle origins lie outside this arc (e.g., M. iliotibialis 1 cranially; M. caudofemoralis longus caudally; Fig. 3), we find such assumptions questionable, especially as the lengths of those muscle fibers are uncertain (Hutchinson 2004b) and so it cannot presently be tested whether further motion was impossible.

Our findings support the inference of Romer (1923) and Hutchinson and Gatesy (2000) that the ''adductor'' muscles (ADD1 and ADD2; Fig. 4) were rather mainly hip extensors in dinosaurs (including *T. rex*). This is because the long ischia increased many muscle moment arms for hip extension, and the adducted limb posture removed some functional requirements (presumably present in basal archosaurs; e.g., Blob and Biewener 2001) for generating large adduction moments during locomotion. In the reference pose (Fig. 2), the M. adductor femoris hip extensor moment arms are 0.50 (ADD2) to 0.39 (ADD1) m. In contrast, the hip adduction moment arms for these muscles are only 0.09 and 0.10 m respectively. This, as expected, is opposite the pattern in more basal reptiles such as crocodylians and lizards (e.g., Blob and Biewener 2001: Fig. 2, Table 1), which seem to have larger moment arms for hip adduction than for extension. Likewise as expected, in our model most muscles that should have originated from the ventral pelvis (e.g., in order of increasing hip adduction moment arms from roughly 0.02 to 0.22 m: FTI1, FTI3, ISTR, and PIFE1–3) in *Tyrannosaurus* had adduction moment arms at most hip joint angles, but these were usually smaller than the hip extensor moment arms. It is possible that in some but not all possible poses Mm. puboischiofemorales externi (PIFE1–3) or M. ischiotrochantericus (ISTR) had larger moment arms for adduction than for flexion or extension respectively, as Charig (1972) inferred.

The conclusions of other studies of the hip abduction capacity of dinosaur pelvic muscles are likewise supported. For example, we reconstructed the deep dorsal thigh muscles M. iliotrochantericus caudalis (ITCA, ITCP) and M. iliofemoralis externus (IFE) as having fairly large hip abduction moment arms (roughly
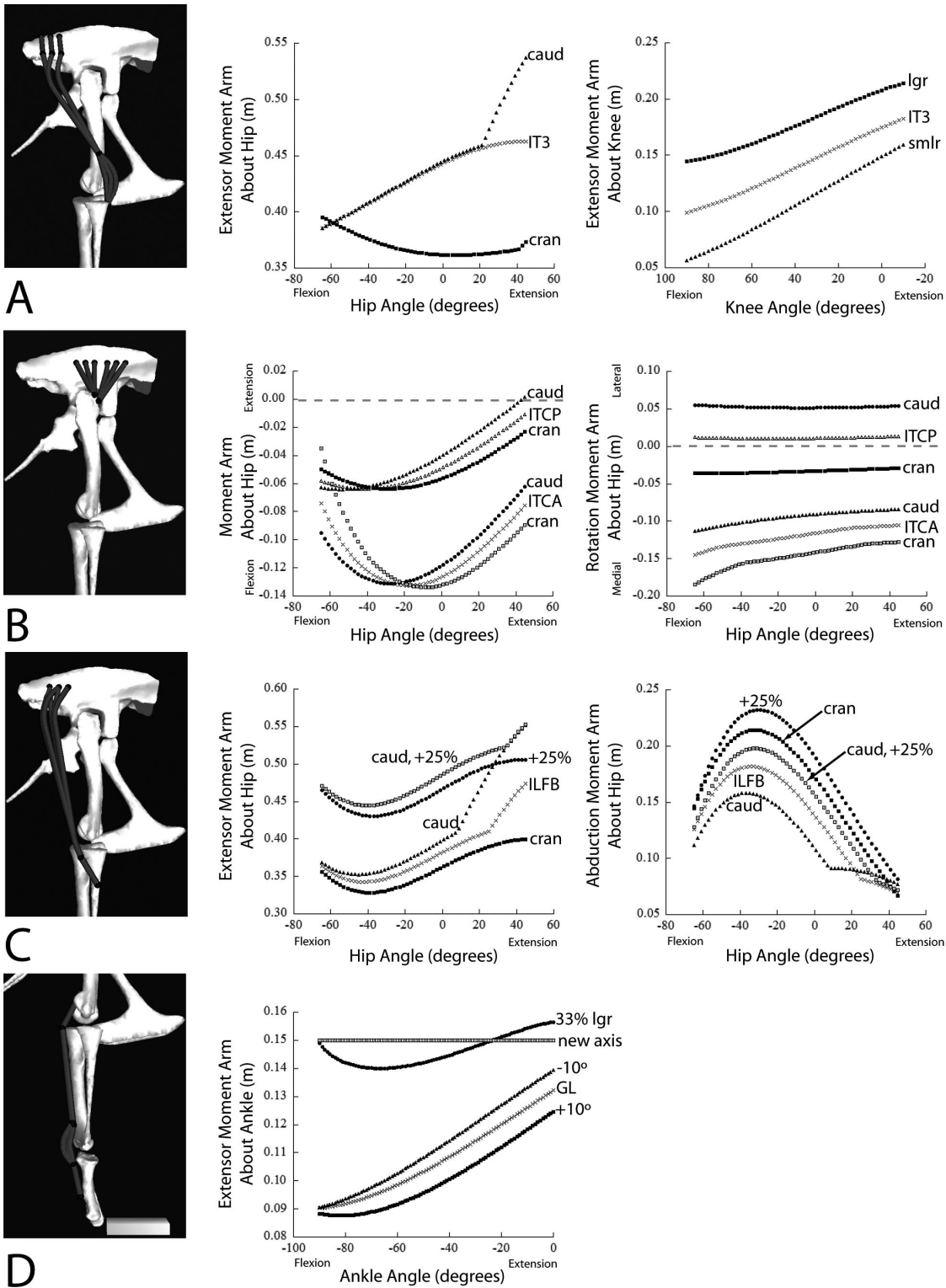
FIGURE 7.   Example sensitivity analysis for several key muscles in *Tyrannosaurus rex*, showing the effects of uncertainty about muscle paths for calculating muscle moment arms. See text for details. A, M. iliotibialis 3 (IT3) pelvic origin and knee extensor wrapping surface; hip (on left) and knee (on right) extensor moment arms plotted against hip or knee joint angle as in Figures 4A, 6A. ''cran'' and ''caud'' indicate the effects of moving the IT3 origin 0.10 m cranially
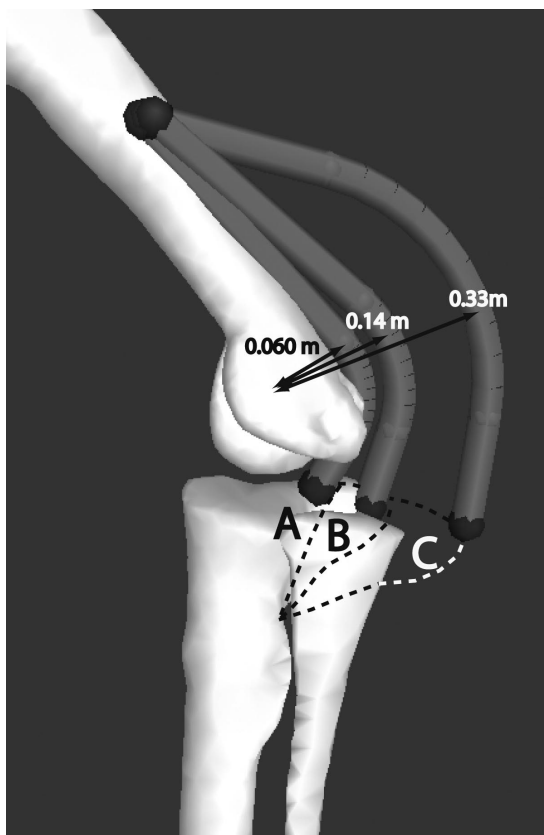
FIGURE 8. Three different muscle-tendon paths for M. femorotibialis externus (FMTE) in *Tyrannosaurus rex* and their biomechanical consequences in this pose (knee angle 45°). Lacking a cnemial crest (A), the knee extensor moment arm might have been as low as 0.040 m. With reasonable assumptions about wrapping surfaces and actual dimensions of the cnemial crest (B), the moment arm would be 0.14 m. In order to reach extreme allometric dimensions (0.33 m knee extensor moment arm), needed to maintain support capability at the same level, the cnemial crest would need to be inordinately large (e.g., C; 0.37 m radius wrapping surface), which it is not. Hence *T. rex* did not have an extraordinarily large knee extensor moment arm.

0.15, 0.19, and 0.26 m) at most joint angles, as many researchers such as Walker (1977), Welles (1986), Carrano (2000), and Hutchinson and Gatesy (2000) inferred. This result should come as no surprise, as these muscles originate dorsal to the hip joint so it would be difficult or impossible for such muscles to switch to exerting adduction moments unless the femur was strongly adducted (medial to the acetabulum), which osteological constraints presumably prevented (e.g., Charig 1972; Paul 1988; Hutchinson and Gatesy 2000). Mm. iliotibiales 1–3 (also M. iliofibularis; Fig. 7C) also had large abduction moment arms: ranging from 0.15 to 0.25 m for IT1–3; highest for IT2P and lowest for IT1 in the reference pose. Again, these findings are sensitive to our assumptions about muscle paths (Fig. 7C), because the moment arms depend on the 3-D paths of muscles from their origins (medially) to their insertions (laterally). Finally, some authors such as Perle (1985) have discussed other functions such as ''hip fixation'' for the deep dorsal thigh muscles (M. iliofemoralis; M. puboischiofemoralis internus). We prefer to consider only muscle functions in modern biomechanical terms, i.e., about the three joint axes (flexion/extension, abduction/adduction, medial/lateral rotation). Thus hip abduction is favored over fixation or other terms for the action of the latter muscles. Few dinosaur studies have discussed medial/lateral long-axis rotation. Hutchinson and Gatesy (2000) inferred that the medial rotation function of M. iliotrochantericus caudalis was important for limb function during the transition from basal dinosaurs to birds, and our analysis supports their inference that this muscle group had a role in that function (Fig. 7B).

←

and caudally; ''lgr'' and ''smlr'' indicate a change of the radius of the knee wrapping cylinder by ±25%. B, M. iliotrochantericus caudalis (anterior and posterior parts; ITCA and ITCP) origins; hip flexor moment arm (on left; as in Fig. 4B) and medial/lateral rotation moment arms (on right) plotted against hip joint angle. ''cran'' and ''caud'' indicate the effects of moving the ITCA or ITCP origin 0.10 m cranially and caudally. C, M. iliofibularis (ILFB) origin; hip extensor moment arm (on left; as in Fig. 4B) and hip abduction moment arm (on right) plotted against hip joint angle. ''cran'' and ''caud'' indicate the effects of moving the ITCA or ITCP origin 0.10 m cranially and caudally; ''+25%'' refers to enlarging the ankle wrapping cylinder radius by 25%. D, M. gastrocnemius lateralis (GL) wrapping surface; ankle extensor moment arm plotted against ankle joint angle as in Fig. 5C. ''+10°'' and ''−10°'' are cases in which the wrapping cylinder was rotated about its y-axis (negative = lateral rotation); ''33% lgr'' involved expanding the cylinder radius by 33%, and ''new axis'' had the wrapping cylinder translated 0.06 m distally to align it with the joint axis rather than the astragalar condyles.

TABLE 6.   Extensor muscle moment arms for *Tyrannosaurus rex*. Results from our analysis compared with values assumed in Hutchinson 2004b abd scaled values from extant taxa (to 6000 kg body mass; from left to right using data from antelope, running birds, mammals, and kangaroos respectively). To calculate the mean moment arms for our initial model, we only used muscles with mean extensor moment arms (see Table 5; Fig. 6). Although probably slightly inaccurate because mean moment arms should be weighted by the physiological cross-sectional area of the muscles (e.g., Biewener 1989), the area of these muscles in *T. rex* is quite uncertain and hence such weighting is difficult. However, dissections of extant taxa (Hutchinson 2004a) show that this error is generally small: weighted moment arms are usually within 10% of mean unweighted moment arms. The joint angles entered were the same as the initial model in Hutchinson and Garcia 2002; based on Paul 1988; generally larger values would be obtained for more extended joints. See text for discussion.

Mean moment arms	This study	Hutchinson (2004b)	Alexander (1977)	Maloiy et al. (1979)	Alexander et al. (1981)	Bennett and Taylor (1995)
Hip extensors	0.38	0.37				
Knee extensors	0.14	0.22	0.12	0.32		
Ankle extensors	0.09	0.12	0.23	0.22	0.26	0.59
Toe flexors	0.10	0.07		0.15		

Muscle Moment Arms and Running Ability.— The average joint extensor moment arms estimated here for a more realistic 3-D musculoskeletal model of *Tyrannosaurus rex* are generally (particularly for the knee and ankle joints) lower than those assumed by Hutchinson and Garcia (2002; also Hutchinson 2004b), especially in more crouched poses, as expected (Tables 5, 6). Entering these values (calculated for the appropriate joint angles) into the models developed by the former authors supports their conclusions about the lack of fast running capability in *T. rex*. The muscle masses needed to support fast running are proportional to the extensor moment arms assumed. Thus the revised moment arms for the extensor muscles acting about the hip, knee, and ankle joints change the extensor muscle masses needed for fast running respectively by a factor of 0.97, 1.6, and 1.3 times, to 9.5, 4.2, and 11% of body mass for the initial ''*T. rex*_1'' model from Hutchinson (2004b). The more upright poses modeled in the latter study, such as model ''*T. rex*_upright'' from Hutchinson (2004b), would have had higher moment arms than the more crouched initial model, so entering the appropriate moment arms for those joint angles only changes the muscle masses for the hip, knee, and ankle joints by a factor of 0.95, 1.2, and 1.1 times. These amendments would not qualitatively change the conclusions of Hutchinson and Garcia (2002) or Hutchinson (2004b); rather, they strengthen those conclusions. They also reinforce our inference that

more upright (but probably not completely columnar as in the reference pose; see Fig. 6) poses are biomechanically more reasonable for *T. rex*. By bolstering the conclusions of Hutchinson and Garcia (2002; also Hutchinson 2004b), our findings cast additional doubt on the idea that *T. rex* could run at extraordinary speeds around 20 m s^{-1} (Bakker 1986; Paul 1988, 1998).

Future Directions.—Our approach is appropriate for modeling musculoskeletal function in the limbs (or almost any system of muscles, bones, and joints) of any vertebrate, and its usefulness in conducting sensitivity analysis is a powerful tool for unraveling the intricacies of locomotion in extinct taxa. Controversies about bipedalism in pterosaurs, locomotor evolution in early tetrapods, forelimb function in dinosaurs (including stance and gait in ceratopsian dinosaurs or the evolution of flight in theropods), or how sauropod dinosaurs could have supported their immense bulk would benefit from similar approaches. One of our most robust conclusions is that limb orientation has a profound influence on limb muscle mechanics, changing their moment arms and hence moment-generating capacity. A direct benefit of initial models like ours is that they form a crucial foundation for dynamic models that can provide deeper insights into the physics of locomotor function, including data on muscle-tendon and ground reaction forces. Without this basic anatomical and geometrical framework, more complex biomechanical models are limited in their

scope and potential research applications. Our results underscore the importance of a circumspect, mechanically sound, and cautiously quantitative approach for inferring muscle function and for comparing the mechanics of animals (extant or extinct) of different sizes and anatomies.

Acknowledgments

Literature Cited

Alexander, R. Mc N. 1977. Allometry of the limbs of antelopes (Bovidae). Journal of Zoology 183:124–146.

Alexander, R. Mc N., A. S. Jayes, G. M. O. Maloiy, and E. M. Wathuta. 1981. Allometry of the leg muscles of mammals. Journal of Zoology 194:539–552.

An, K. N., K. Takahashi, T. P. Harrigan, and E. Y. Chao. 1984. Determination of muscle orientations and moment arms. Journal of Biomechanical Engineering 106:280–283.

Arnold, A. S., and S. L. Delp. 2001. Rotational moment arms of the medial hamstrings and adductors vary with femoral geometry and limb position: implications for the treatment of internally rotated gait. Journal of Biomechanics 34:437–447.

Arnold, A. S., S. Salinas, D. J. Asakawa, and S. L. Delp. 2000. Accuracy of muscle moment arms estimated from MRI-based musculoskeletal models of the lower extremity. Computer Aided Surgery 5:108–119.

Bakker, R. T. 1986. Dinosaur heresies. William Morrow, New York.

———. 2002. Speed in tyrannosaurs. Journal of Vertebrate Paleontology 22(Suppl. to No. 3): 34A.

Bennett, M. B., and G. C. Taylor. 1995. Scaling of elastic strain energy in kangaroos and the benefits of being big. Nature 378: 56–59.

Biewener, A. A. 1989. Scaling body support in mammals: limb posture and muscle mechanics. Science 245:45–48.

———. 1990. Biomechanics of mammalian terrestrial locomotion. Science 250:1097–1103.

Blanco, R. E., and G. V. Mazetta. 2001. A new approach to evaluate the cursorial ability of the giant theropod *Giganotosaurus carolinii*. Acta Palaeontologia Polonica 46:193–202.

Blob, R. W. 2001. Evolution of hindlimb posture in nonmammalian therapsids: biomechanical tests of paleontological hypotheses. Paleobiology 27:14–38.

Blob, R. W. and A. A. Biewener. 2001. Mechanics of limb bone loading during terrestrial locomotion in the green iguana (*Iguana iguana*) and American alligator (*Alligator mississipiensis*). Journal of Experimental Biology 204:1099–1122.

Brown, N. A. T., M. G. Pandy, W. L. Buford, C. E. Kawcak, and C. W. McIlwraith. 2003a. Moment arms about the carpal and metacarpophalangeal joints for flexor and extensor muscles in equine forelimbs. American Journal of Veterinary Research 64:351–357.

Brown, N. A. T., M. G. Pandy, C. E. Kawcak, and C. W. McIlwraith. 2003b. Force- and moment-generating capacities of muscles in the distal forelimb of the horse. Journal of Anatomy 203:101–113.

Bryant, H. N., and K. L. Seymour. 1990. Observations and comments on the reliability of muscle reconstruction in fossil vertebrates. Journal of Morphology 206:109–117.

Buford, W. L., Jr., F. M. Ivey Jr., J. D. Malone, R. M. Patterson, G. L. Peare, D. K. Nguyen, and A. A. Stewart. 1997. Muscle balance at the knee—moment arms for the normal knee and the ACL-minus knee. IEEE Transactions on Rehabilitation Engineering 5:367–379.

Carrano, M. T. 2000. Homoplasy and the evolution of dinosaur locomotion. Paleobiology 26:489–512.

Carrano, M. T., and J. R. Hutchinson. 2002. Pelvic and hindlimb musculature of *Tyrannosaurus rex* (Dinosauria: Theropoda). Journal of Morphology 252:207–228.

Charig, A. J. 1972. The evolution of the archosaur pelvis and hindlimb: an explanation in functional terms. Pp. 121–151 *in* K. A. Joysey and T. S. Kemp, eds. Studies in vertebrate evolution. Oliver and Boyd, Edinburgh.

Christiansen, P. 1999. Long bone scaling and limb posture in non-avian theropods: evidence for differential allometry. Journal of Vertebrate Paleontology 19:666–680.

Colbert, E. H. 1964. Relationships of the saurischian dinosaurs. American Museum Novitates 2181:1–24.

Delp, S. L., and J. P. Loan. 1995. A graphics-based software system to develop and analyze models of musculoskeletal structures. Computers in Biology and Medicine 25:21–34.

———. 2000. A computational framework for simulating and analyzing human and animal movement. IEEE Computing in Science and Engineering 2:46–55.

Delp, S. L., and F. E. Zajac. 1992. Force- and moment-generating capacity of lower-extremity muscles before and after tendon lengthening. Clinical Orthopaedics 284:247–259.

Delp, S. L., J. P. Loan, M. G. Hoy, F. E. Zajac, E. L. Topp, and J. M. Rosen. 1990. An interactive graphics-based model of the

and M. G. Lockley, eds. Dinosaur tracks and traces. Cambridge University Press, Cambridge.

———. 1990. Dinosaur tracks. Chapman and Hall, London.

Van der Helm, F. C., H. E. Veeger, G. M. Pronk, L. H. Van der Woude, and R. H. Rozendal. 1992. Geometry parameters for musculoskeletal modelling of the shoulder system. Journal of Biomechanics 25:129–44.

Van Leeuwen, J. L. 1992. Muscle function in locomotion. Advances in Comparative and Environmental Physiology 11:191–250.

Walker, A. D. 1977. Evolution of the pelvis in birds and dinosaurs. Pp. 319–358 *in* S. Mahala Andrews, R. S. Miles, and A. D. Walker, eds. Problems in vertebrate evolution (Linnean Society Symposium Series 4).

Welles, S. P. 1986. Thoughts on the origin of the Theropoda. Pp. 31–34 *in* K. Padian, ed. The beginning of the age of dinosaurs. Cambridge University Press, Cambridge.

Witmer, L. M. 1995. The extant phylogenetic bracket and the importance of reconstructing soft tissues in fossils. Pp. 19–33 *in* J. J. Thomason, ed. Functional morphology in vertebrate paleontology. Cambridge University Press, Cambridge.

Zajac, F. E. 1989. Muscle and tendon: properties, models, scaling, and application to biomechanics and motor control. Critical Reviews in Biomedical Engineering 17:359–411.

Appendix 1

Bone Geometry Acquisition

We used a digitizing apparatus (Freepoint 3-D Sonic Digitizer; GTCO CalComp, Columbia, Maryland) to sample the (x,y,z) surface coordinates of each bone, and AutoCAD 12 (Autodesk, Inc., San Rafael, California) software to construct a. dxf format (CAD-specific) polygonal mesh connecting those points. Masking tape was stretched over the bones following their main contours in lines about 5–20 cm apart (depending on the density of points desired; a higher density was used in more crucial areas such as joint surfaces and trochanters), and a permanent marker was used to mark points to digitize every 1 cm along the tape. The tape was positioned so as to (by our subjective impression) best represent the overall contours of the bone (Fig. 1). The points along the tape were then digitized.

The. dxf mesh images were processed in Alias|Wavefront Studio 8.5 to replace the rough polygonal mesh with a more aesthetically appealing and biologically realistic NURBS model (splines as cross-sections through the bones, positioned along the masking tape lines), which smoothed out the contours of the bone images. In a few crushed regions of some bones (ilium, femoral and tibial shafts), paper or cardboard was smoothly placed over the crushed area to maintain the continuity of the bone surface during digitizing. Only the ventrolateral surfaces of the right ilium of MOR 555 were digitized, as the medial surface of the ilium was still embedded in the jacket and inaccessible, but measurements of the mediolateral bone thickness were taken. A few missing pieces of the iliac blade were reconstructed by scaled comparison with other *Tyrannosaurus* ilia. Part of the iliac peduncle of the right pubis was missing, but was not crucial to have in the model. Except for some mediolateral flattening proximally, the pubes were otherwise in good condition. The right ischium was deformed (distal end artifactually curved), but most of these deformities were easily removed by adjusting the positions of the splines to straighten out its shaft. The shaft of the MOR 555 femur is crushed (Farlow et al. 1995) so the splines were deformed to eliminate the crushing and return the femur shaft cross-section to a more regularly rounded shape. The fibular condyle (''ectocondylar tuber'') of the right femur was also broken off, so the intact condyle from the left femur was molded in modeling clay and digitized, then mirrored from the left to the right side of the body. The other bones

were in reasonably good condition, requiring only minor smoothing of edges. Most of these alterations to the original bone images were done simply for aesthetic reasons and would have negligible effects on our results. The tibia, fibula (oriented to the tibia by the positions of the proximal tarsals, cnemial crest, tibial plateau, and tibiofibular crest), and astragalus were articulated (the calcaneum was deemed unnecessary for our purposes, but measurements were taken for reference) and joined into one ''tibiotarsus'' bone file, whereas the distal tarsals and metatarsals II-IV (again, metatarsals I and V were omitted for simplicity, but measured for reference) were joined as a ''tarsometatarsus.'' All bones on the right side were mirrored about the midsagittal plane to produce identical bones for the left limb (not shown; optional).

The splines were then combined (to give them a single continuous surface) and converted back to a point cloud. These data were exported as Inventor (.iv) files and converted into the required bone file format (.asc) for the biomechanical model (see main text). The resulting bone files generally had too many polygons for rapid 3-D graphics rendering (100,000–500,000 triangular polygons), so a final step was used to decimate them into more manageable files of 5000 (femur), 4000 (tibiotarsus; tarsometatarsus), 3000 (pubes), or 2000 (ilium; ischium) polygons. This procedure involved first removing coincident points and other points that were extremely close together from the cloud, and second passing the data through a decimation algorithm (based on Schroeder et al. 1992) that iteratively removed points having minimal or redundant importance for surface geometry.

Appendix 2

Joint Axis Estimation

The ilium, ischium, and pubis were combined into a single ''pelvis'' segment, with the x-axis oriented cranially, the y-axis oriented dorsally, and the z-axis oriented laterally (these are the positive directions of the axes, used similarly for all segments except for the toes, which had the x and y axes switched, as appropriate). The center of the acetabulum was found by selecting bone vertices within the arch of the acetabulum. We then aligned a plane through the acetabulum (this plane was parasagittal and positioned in the mediolateral center of the acetabulum), projected the bone vertex coordinates onto the plane, and fit a circle to the projected points using the MATLAB (The Mathworks, Inc., Version 6.5, 2002) optimization toolbox. The center of the hip joint (0,0,0 in x,y,z coordinates) was the center of the circle. A sphere was then fit to the femoral head to find its center of rotation. The origins of these bones were matched to this center, forming the hip joint (using the Euler/Cardan method).

For the knee joint, the tibia was first manually aligned to articulate with the distal femur using three criteria: (1) medial side of the tibial crest in the same longitudinal plane as the medial femoral condyle (i.e., femoral condyles centered mediolaterally on top of the tibia); (2) caudal edge of the lateral femoral condyle located just proximal to the caudal edge of the lateral side of the tibia (i.e., femoral condyles centered craniocaudally on top of the tibia); and (3) flexor fossa of the proximal tibia aligned distal to the popliteal fossa of the femur, and extensor canal of the distal femur aligned proximal to the cnemial crest (i.e., ensuring that knee flexor and extensor tendons followed a straight proximodistal line across the joint at 0° varus/valgus). Next, vertices along the fibular and tibial (medial and internal) condyles of the femur were identified in a line following the main curvature of each condyle, and this curved line was projected onto a longitudinal (sagittal) plane cutting through each of the two condyles, parallel to their curvature. Circles were fit to the projected points using the MATLAB optimization tool-

box. The knee axis of rotation was then defined as the line connecting the centers of those two condylar curves, and the knee joint center was defined as the midpoint of that line. For simplicity, translation of the tibia with respect to the femoral condyles is not included in our initial model but could be added to future versions. The center of rotation of the knee joint (for flexion/extension) hence was fixed rather than represented as a mobile ''instant center of rotation'' or ''screw-home mechanism,'' an approach that matches recent biomechanical representations of human knee function through much of the range of knee flexion/extension (e.g., Eckhoff et al. 2003). Our conclusion that knee extensor moment arms should have increased with knee extension would be unlikely to change greatly with addition of joint axis translation; a decrease of slope might be expected at large angles of knee flexion. This is supported by experimental data for humans in which inclusion of joint translation still results in a maximal extensor moment arm occurring at/near full knee extension (e.g., Spoor and van Leeuwen 1992; Buford et al. 1997; Krevolin et al. 2004). This procedure objectively positions the knee joint center without making overly speculative assumptions about articulations. The ankle joint axis was determined by the same procedure, using the lateral and medial condyles of the astragalus (presuming approximate similarity with the calcaneum), and the metatarsophalangeal joint axis was found by using the medial and lateral curvatures of the distal end of the third metatarsal.

To account for the thickness of soft tissues between the joints, the bones were displaced slightly apart from each other. The hip joint was not moved, because its center was already in the middle of the acetabulum, leaving much room for ligaments and other hip joint tissues (note that the radius of the femoral head was only 0.10 m, whereas the acetabular radius was 0.15 m, leaving about 50% of the acetabulum free for soft tissues; quite unlike a typical extant bird with a tighter bony hip socket [Hotton 1980]). Considering initial measurements from extant archosaurs, we added an additional 7.5% to the length of the femur, 5% to the tibiotarsus, and 10% to the metatarsus to accommodate cartilages and other soft tissues such as the foot pad beneath metatarsal 3.

The joints were all treated as simple hinges with one degree of freedom (flexion/extension) except for the hip joint, which was modeled as a ball-and-socket (gimbal) joint with three degrees of freedom: abduction/adduction (about the x-axis), medial/lateral rotation (about the y-axis), and flexion/extension (about the z-axis). The joint was defined as three successive body-fixed rotations of the femur with respect to the pelvis in the order rx, ry, rz; the remaining joints were defined similarly. The joint between the ground and the pes (termed the ''foot'' joint) was allowed to roll mediolaterally independent of the flexion/extension of the metatarsophalangeal joint. Thus the limb had a total of ten degrees of freedom; an additional degree of freedom can be added or removed, depending on the complexity desired for the foot, to represent the interphalangeal hinge joint of digit 3, phalanx 1 (dividing the pes segment into lengths of 0.224 and 0.360 m, proximally and distally in the pes).

Zero degrees of rotation in flexion/extension (here called the fully columnar pose) was defined as having the limbs oriented in a straight line perpendicular to all the joint axes of the limb. Note that because of our axis definitions, the metatarsophalangeal joint angle was 0° when the phalanges were at 90° to the metatarsus in the sagittal plane. For the default pose, the hip abduction angle was set at 10° to keep the femur clear of the pelvis and trunk (as in most reconstructions [e.g., Osborn 1913, 1916; Paul 1988]), and this slight abduction was maintained in all poses modeled here unless otherwise noted. To then bring the lower limb back medially (matching theropod dinosaur footprints and osteology; Molnar and Farlow 1990; Thulborn 1990), the tibiotarsus segment was given 15° of valgus (adduction),

which also remained constant in the model unless otherwise noted. This angulation left the lateral femoral condyle with noticeably more space between it and the tibial plateau than for the medial femoral condyle, so perhaps a larger meniscus was present there (likely, judging from extant taxa [personal observation]), or the fibula was markedly more proximally positioned than bone articulations suggest (contraindicated by fossils [e.g., Osborn 1916; Lambe 1917; personal observation]).

Appendix 3

Muscle Reconstruction

We omitted the intrinsic pedal muscles (because of their small size and uncertain anatomy [Hutchinson 2002]) and M. popliteus (because the knee joint was treated as a simple hinge, thus this muscle has no function in the model). M. iliotibialis 2 was divided into preacetabular ''IT2A'' and postacetabular ''IT2P'' portions because of its large expanse and slight or complete subdivision among extant archosaurs. Similarly, considering its apparent large size, M. iliotrochantericus caudalis (ITC) was split into cranial ''ITCA'' and caudal ''ITCP'' subheads. The distal secondary tendons of M. ambiens (past the cnemial crest of the proximal tibia, joining the digital flexors) and M. fibularis longus (past the lateral condyle of the distal tibia, joining the digital flexors) were modeled as muscles separate from their proximal muscle bellies and tendons to allow for independent action about the knee/ankle and toe joints. The presence or absence of some parts of the ''hamstring'' flexor cruris complex is ambiguous for dinosaurs (Carrano and Hutchinson 2002; Hutchinson 2002). We included M. flexor tibialis internus 1 (FTI1) because of the presence of a tubercle on the ischium (Hutchinson 2001a) that might indicate the origin of that muscle (Carrano and Hutchinson 2002), but the possibility that this muscle head was absent (and M. flexor tibialis internus part 4, presumed to be absent) warrants consideration in studies that examine whole-limb function. Details concerning the internal architectural and physiological characteristics of the muscles (e.g., optimal fiber length, pennation angle, maximum shortening velocity), although included in many models of extant animals, were not included in the model for the sake of simplicity, as there is a paucity of reliable data for many of these parameters in theropods (Hutchinson 2004b) and, furthermore, the values of these parameters would have had little bearing on our procedures for reconstructing muscle paths and moment arms.

Appendix 4

Muscle Path Specification

Axes (x,y,z) referred to here and in Table 4 are the segment axes, not joint axes. For the hip flexor/extensor muscles, a key problem was preventing muscles with origins that were furthest craniad/caudad on the pelvis (or vertebral column) from following paths through spaces that in life would have been filled by other muscles that were closer to the hip joint. As a first step to solve this problem, we restricted the lines of action of the IT1, IT3, ILFB, PIFI1–2, FTE, CFB, and CFL to areas cranial or caudal to the acetabulum, using cylindrical wrapping surfaces of various radii and positions (Table 3). The choice of these radii and positions had to be arbitrary based on a subjective consideration of proximity to neighboring muscles, bones, and joints, and how curved the muscle path should appear.

To prevent the lines of action of other pelvic muscles from cutting through pelvic bones in certain joint angles, we inserted elliptical wrapping surfaces centered on the hip joint (Table 4). The purpose of these wrapping surfaces was to represent the physical bone surfaces, which the model could not otherwise constrain muscles from penetrating. In all cases and poses, we

checked the model to ensure that muscles were not penetrating bones.

Via points were included in many of the muscles to constrain their paths through particular points, especially close to grooves where tendons would have slid through. The M. iliotibialis muscles (IT1–3) had via points near the knee extensor groove on the distal femur (Fig. 3A), with additional proximal points added to help most of these muscles remain clear of the ilium at all joint angles. M. ambiens (AMB) also had a via point near the extensor groove, and its distal secondary tendon had additional points to keep it on a course to join the digital flexors (Fig. 3-D). A via point for M. iliofibularis at the proximal tibiotarsus kept the line of action close to the knee joint, simulating the presence of soft tissues (e.g., other muscles) caudal to it. M. puboischiofemoralis externus 1 and 2 (PIFE1, PIFE2) each had a via point close to the pubic origin and the femoral insertion to maintain their path and prevent the muscles from cutting through bones (Fig. 3B). M. ischiotrochantericus (ISTR) needed two extra pelvic and one femoral via points to constain its convoluted line of action. The lower limb muscles all had via points along their lines of action to keep them parallel to the bones as necessary, and to keep their origins from moving too far through/away from bony landmarks revealing their courses (Fig. 3C,D).

The knee extensor muscles used cylindrical wrapping surfaces centered on the knee joint z-axis of the femur, with a radius of 0.265 m (for IT1), 0.23 m (for IT2A and IT2P), or 0.20 m (for IT3, AMB, FMTE, and FMTI). Like all other non-avian (indeed, non-ornithurine) dinosaurs, *Tyrannosaurus* lacked a patella so this assumption is justifiable, as the knee extensor tendons follow a similarly curved path in extant outgroups lacking a patella (e.g., crocodiles, turtles). The radii were estimated from radii of the medial (0.13 m) and lateral (0.11 m) femoral condyles (mean = 0.12 m), the size of the extensor canal on the distal femur (radius 0.06 m, for the deeper part of the extensor tendon), and the prominence of the tibial cnemial crest (0.13 m long from its cranial tip caudally to the cranial end of the tibial plateau), with the most superficial muscles given the wrapping cylinders with the largest radii. This estimation of the wrapping surface sizes accounted for the thickness of the components of the knee extensor tendon as well as articular cartilages of the knee joint. The knee extensor wrapping cylinders were rotated $-10°$ (laterally) to keep the muscles from sliding too far medially during knee extension. Likewise, the knee flexors (ILFB, FTI1, FTI3, FTE) were given a cylindrical wrapping surface of 0.20 m radius (translated 0.05, -0.07, and 0.02 m in the x,y,z directions) on the femur to restrict them from moving cranially too close to (or through) the knee joint, given that ankle extensor muscles would have occupied space in this region.

At the ankle joint, the ankle extensor muscle paths were prevented from cutting through the ankle bones or switching from extension into flexion by inserting cylindrical wrapping surfaces into the model, connected to the tibiotarsus segment. Mm. gastrocnemii were given a wrapping cylinder radius of 0.15 m, whereas the deeper digital flexor muscles all had a wrapping cylinder radius of 0.11 m. These radii were calculated by measuring the radius of the tibiotarsal condyles (medial: 0.089 m; lateral: 0.064 m; mean: 0.077 m) and increasing that value by 100% for the presumably large ''Achilles tendon'' of Mm. gastrocnemii or 50% for the digital flexor muscles to account for the thickness of those tendons crossing the ankle joint and any interposed articular cartilage. These 50–100% expansions of moment arms by soft tissues are upper-end relative values from our inspections of extant animal limb joints (e.g., ground birds such as ostriches, emus, chickens, and turkeys). Another cylinder (radius 0.07 m; x,y,z translation -0.04, -0.02, 0.003 m) was used as a wrapping surface for the tendon of M. fibularis longus across the ankle joint.

The toe joint flexors wrapped around a cylinder of radius 0.10 m (translated 0.11, 0.0, and -0.02 m in the x,y,z directions), matched to the radius of the distal end of the third metatarsal plus 100% to account for articular cartilage and tendon thickness; again based on dissections of extant taxa. A similar cylinder of radius 0.09 m (not translated away from the toe joint axis) was used as a wrapping surface for the toe extensors, attached to the origin of the pes segment.